Tethered Payload Control from an Autonomous Helicopter

James E. May

Thesis submitted to the Faculty of the

Virginia Polytechnic Institute and State University

in partial fulfillment of the requirements for the degree of

Master of Science

in

Mechanical Engineering

Kevin B. Kochersberger, Chair

Al Wicks

Steve Southward

August 09, 2010

Blacksburg, Virginia

Keywords: Robotics, Unmanned Systems, Tethered Payloads

Tethered Payload Control from an Autonomous Helicopter

James E. May

ABSTRACT

A system is designed to deploy and support a tethered ground robot from an autonomous helicopter. A winch is designed and built. Electrical hardware for power distribution and control are designed. Several applied controls problems are investigated. A control architecture is established and low level controllers are designed to meet the demands of two higher level algorithms. A tether tension controller is designed to avoid the danger of excess slack in the tether interfering with the robot's mobility. A payload sway damping controller is investigated and simulated. Its is shown to be effective in damping dangerous payload oscillations by modulating the vertical manipulation of the winch during hoisting. Future design recommendations are given regarding improvements for a second design iteration.

Acknowledgments

I'd like to thank all of those who in one way or another made this project possible. First and foremost, thanks are due to Dr. Kevin Kochersberger, who gave me the opportunity to join his design team. Dr. K, thanks for the opportunity and the friendship. Each of my committee members has contributed significantly to my education. Dr. Steve Southward provided me with the Controls background necessary to undertake this project. Dr. Al Wicks has inspired in me a keen interest in Instrumentation and Signal Processing, and I appreciate and enjoyed and the opportunity to work on his team.

I'd be remiss not to thank all of my colleagues at the Virginia Tech Unmanned Systems Lab. Dan Hager, Eric Brewer, Mike Rose, Prather Lanier, Eric Gustafson, and Nathan Short have all helped my in some capacity. More importantly, they've been great friends. A special thanks is due to Brian McCabe, who helped considerably in conducting hardware tests. Brian will continue this work in pursuit of his thesis. John Bird has always taken the time to answer my questions willingly and knowlegably. Kevin Stephanik was tremendously helpful with electrical design.

I'd like to thank my family, for whom I am very grateful. I couldn't ask for better parents. I'm very blessed to have three great sisters, whom I am very proud of. Mom, Dad, Amy, Mary Jane, Grace, I love you.

Finally, Laura. Thanks for being so patient and supportive. I love you.

Contents

List of Figures

List of Tables

Chapter 1

Introduction

This thesis examines the problem of deploying a tele-operated robot from an autonomous helicopter. The applications cover a wide range of scenarios, including post disaster sampling. This thesis includes design and analysis of a payload deployment system, design and implementation of a tether tension controller to minimize tether slack, and simulation of an experimental payload sway controller.

1.1 Motivation

As robot technology rapidly expands, the use of robots to execute tasks which are dangerous or difficult for human beings is becoming commonplace. The state of the art in tele-operation of Unmanned Aerial Vehicles (UAVs) and Unmanned Ground Vehicles (UGVs) allows for

Figure 1.1: Virginia Tech's Yamaha RMAX UAV

long distance, non-line-of-sight control. Even with the tremendous capabilities of these unmanned systems, there are limitations. Tradeoffs between operating range, endurance, size, manuverability, and precision present challenges when devising complex robot missions. Often, these challenges can be overcome when two or more robots cooperate.

There exists a current field of research where robots are deployed into environments uninhabitable to humans in order to collect information about that environment. Many of the robots designed for this type of mission are limited by the traversability of the terrain within the desired operating environment. The Unmanned Systems Laboratory at Virginia Tech is designing a cooperative robot system where a small ground robot fitted for environmental sampling is deployed and retrieved from a Vertical Take Off and Landing (VTOL) UAV. Because the recovery of the ground vehicle is critical to the success of the mission, the UGV

will remain tethered to the UAV during operation. In addition to designing and outfitting functional robotic platforms, the design of a deployment control system is necessary. This thesis will cover the design of a payload deployment system and various control algorithms proposed to ensure mission safety.

The system described in this thesis must be able to execute a semi-autonomous mission which includes deploying a robot within a designated area of interest, obtain samples from that area, and returning the robot to an area where the samples can be safely examined. Virginia Tech's Yamaha RMAX UAV, seen in Figure 1.1, will be outfitted with this system in the future for a tethered robot mission. The RMAX is equipped with a WePilot Automated Flight Control System (AFCS), capable of executing GPS waypoint commands, as well as maintaining a steady hover. This mission will be conducted by a team of ground control operators stationed in a mobile operator control unit (OCU) booth, shown in Figure 1.2. One operator will command the helicopter's Automated Flight Control System while closely monitoring the stability of the UAV. Another operator will be responsible for controlling various payloads, and monitoring health status of the on board power supplies and communication link. A third operator will control the deployment system, and teleoperate the ground robot during its sampling mission. A safety pilot will manually control the helicopter during takeoff, landing, and emergency situations. The multi-robot sampling mission consists of the following steps:

1. With the robot secured in the payload bay, the helicpoter flies to a GPS waypoint identifying a target deployment site.

2. From a hover, the Ground Sampling Robot is safely and accurately deployed.

3. While tracking the robot with the helicopter and maintaining tension on the tether, a sampling mission is conducted.

4. Ground Sampling Robot is hoisted while controlling sway.

5. The system returns to designated landing site.

Figure 1.2: Virginia Tech's mobile Operator Control Station

1.2 Overview of Work

The research which this thesis describes is intended to lay the groundwork for future UAV-tethered payload operations. A first iteration hardware design is built and tested. This

design encompasses all of the necessary elements for a stand alone system. A winch motor and gearhead are selected and evaluated, and an off-the-shelf motor controller is used for closed loop position and speed control. Supporting electronics are built for power distribution, communication and high level control, and feedback instrumentation. Future design recommendations are made regarding potential improvements to the reliability of the system.

A control architecture is established in order to achieve control of two nonlinear systems: tension control of the tether, and sway control of an oscillating payload. These high level controllers require well tuned position and speed controllers to manipulate the system. Speed and position controllers are simulated and implemented on physical hardware. The closed loop system characteristics are evaluated in order to understand the limitations of these controllers.

Tether tension control is achieved by manipulating the position controller. The tension control algorithm uses feedback from a load cell in line with the tether to maintain a desired tension. This system is modeled and implemented on physical hardware. Experimental results are discussed in the context of system performance. Recommendations are made for future implementation of this controller on the RMAX UAV.

Additionally, control methods for reducing payload oscillation during hoist and flight is investigated. The objective of this work is to examine payload sway control methods that employ only the vertical actuation of the tether. The system models are derived in detail, and the open loop system response is simulated. The control laws are derived, and closed

loop damping control is simulated.

Chapter 2

Literature Review

The scope of this thesis covers a broad spectrum of engineering topics as they relate to deploying and supporting a semi-autonomous payload from an autonomous helicopter. Because of this, a variety of technical literature was reviewed to understand the terminology and state of the art of the wide scope of subject matter herein. Some of this literature consists of prior Master's Theses published by colleagues at the Virginia Tech Unmanned Systems Lab, as their research has laid the groundwork for this mission. Other literature covers the much studied problem of suspending a payload from a helicopter platform.

2.1 Tethered Ground Robot Operations

Operation of a ground robot tethered to a helicopter is a central area of research for the Virginia Tech Unamnned Systems Lab. The lab has a variety of unmanned helicopters fitted with controllers for autonomous flight. Historically, the lab has involved a team of mechanical, electrical, and computer engineering graduate and undergraduate students to equip these platforms with a variety of sensors to accomplish difficult missions. This section will review the work published by previous graduate students which directly relates to the ground robot deployment mission. This work includes ground robot design, operator situational awareness, landing zone detection, and vision based payload tracking.

2.1.1 Ground Sampling Robot Mission

Rose's thesis [1] contributes several cornerstone elements to this system. Primarily, he designs a teleoperated robot platform capable of supporting localization and sampling hardware. This robot platform is designed to be deployed from and remain attached to an autonomous helicopter. The platform, depicted in Figure 2.1, features a differential track system for movement and steering. It has a large payload bay to be equipped with a robotic arm and sampling apparatus. The vehicle is controlled remotely from serial commands generated on the Operator Control Unit (OCU), which is to be linked through the helicopter, and passed to an onboard controller.

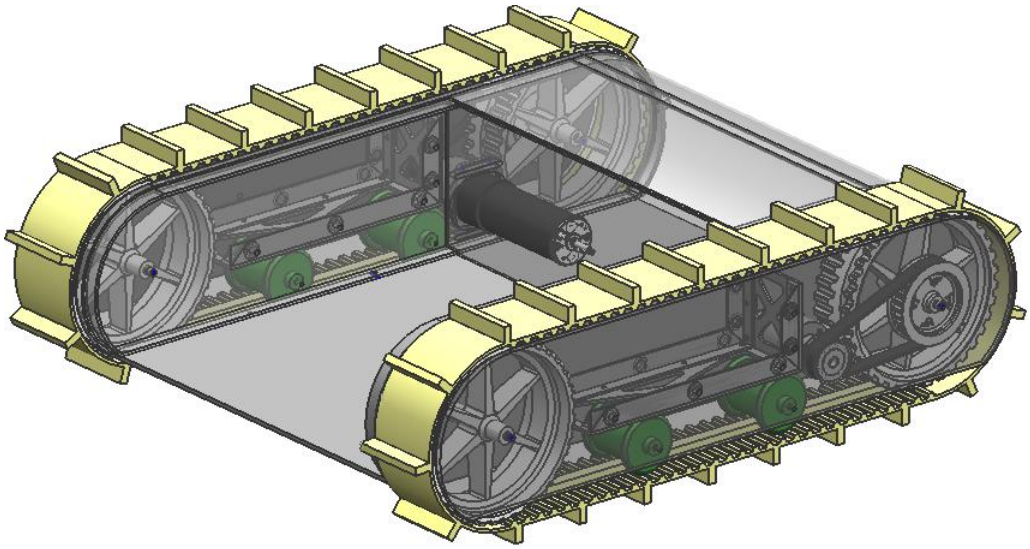

Figure 2.1: Small teleoperated sampling robot designed by Virginia Tech

Additionally, Rose contributes path planning algorithms to determine efficient routes around obstacles. From stereo image data obtained onboard the helicopter, his algorithm filters terrain based on slope and gradient, and calculates efficient paths for an autonomous controller or human operator to navigate. The ability to navigate and accomplish mission objectives quickly and efficiently is critical due to the helicopter's limited endurance.

2.2 Helicopter Slung Load Operations

The lift and mobility characteristics of the helicopter give it the unique ability to hoist, transport, and often precisely place payloads. The use of helicopters to convey slung payloads is a widely studied practice. It has many applications, both military and commercial. The dynamics of the helicopter-slung load system is a complex area of research.

Lucassen and Sterk [2] perform a dynamic stability analysis of a slung load on a hovering helicopter. Three dimensional equations of motion are derived, neglecting aerodynamic loading on the slung load and constraining the helicopter to a vertical plane. The slung load is modeled as a simple pendulum with a single attachment point. Experimental results agree with the simulated stability analysis.

After Lucassen and Sterk, much of the work in this field studies complex models for specific aircraft and specific tether configurations. Because the platform used by Virginia Tech has demonstrated the ability to maintain flight stability with a single tether slung load, this thesis will not cover complex flight dynamics. A more relevant area of research, however, has stemmed from these studies. This is the study of actively damping payload oscillations using robotic platforms.

Bisgaard conducts research in topics relevant to controlling a slung load from an unmanned helicopter. His goal is to support a mine detecting mission, where a tethered sensor is towed a short distance off the ground. A state estimator is developed for payload position with sensor fusion of vision-tracking and inertial data [3]. His algorithm uses an unscented kalman filter, which incorporates nonlinear models of the plant and sensors. A control structure is developed which utilizes feedback to control helicopter motion in a way that reduces payload pendulation [4]. His results are impressive, as pendulation is reduces significantly compared to the open loop system.

Agrawal, et al [5] develop a novel six-cable suspended robot. The robot, which served as

a platform to hold payloads, controls all suspension cables for active damping of sway and accurate payload transportation. Combining the fast manipulation of the cable suspended robot with the cumbersome motion of the helicopter, they are able to achieve more precise control than either system individually [6] .

Rosen, et al [7] develop an active aerodynamic stabilization mechanism for the helicopter-slung load system. This stabilization approach consists of two vertical aerodynamically loaded surfaces for which the angle of incidence is varied by a controller. Angular rates of the helicopter and slung load as well as load acceleration are used in a feedback controller. The results show that this solution is capable of stabilizing the helicopter-slung load system for a wide range of airspeeds.

2.3 Payload Control from Cranes

One of the problems investigated in this thesis is the control of a suspended payload that begins to oscillate. Because this a problem which occurs in handling cranes, a review of control techniques within this field is conducted. Bobasu, et al [8] develop nonlinear algorithms for adaptive control a of handling crane. The crane has a translational actuator which controls the position of a vertical actuator. The algorithm is simulated and the adaptive controller outperforms the simple nonlinear controller.

Yanai, et al [9] use an inverse dynamics calculation for feedback control of a crane. The

crane model has a two axis translational actuator which controls a trolley where a winch is mounted. The control method is used to control a payload to follow a path while minimizing error due to sway. The controller is shown to be effective.

Abdel-Rahman and Nayfeh [10] investigate pendulation reduction in boom cranes using cable length manipulation. The application is a ship mounted boom crane which is excited by oceanic waves. Their strategy involves reeling and unreeling the payload at near-resonance conditions to alter the dynamics. They develop two dimensional and three dimensional models and show their control strategy to be effective in reducing payload pendulation. With the selection of appropriate reeling and unreeling speeds, their control strategy is particularly effective.

Bockstedte and Kreuzer [11] develop a control technique which dampens payload oscillations using only vertical actuation. The technique, called modal coupling control, emulates an elastic pendulum. Two models are introduced: a simple pendulum model, consisting of a single tether, and a flying crane model, with multiple tethers. Both models are effective in reducing oscillations of the suspended payload.

The single tether model is adapted and tested later in this thesis. I find that the controls strategy for emulating the elastic pendulum is dependant on a small angle approximation for pendulum frequency and the absense of aerodynamic damping. Because a real system is subject to aerodynamic damping and may be required to perform in cases of larger angles, this control strategy could be ineffective. An alternative to this control strategy is introduced

in this thesis which does not depend on the small angle approximation. This strategy uses the same principles introduced by Bockstedte and Kreuzer, but is more robust to large pendulation angles.

Chapter 3

Hardware Design of a Tethered Robot Deployment and Recovery System

The tethered robot deployment and recovery system designed for this mission is a self-contained system which mounts to the payload bay of the RMAX. The system is self-powered and contains all necessary electronics for autonomous operation. The system communicates with the ground operator interface over the helicopter's payload radio via a single serial port at a baud rate of 19200 Baud. Several tiers of the control hierarchy such as motor speed and position control, tension control, and hoisting control are embedded. This chapter provides an overview of the system architecture, selection of electro-mechanical components, and design of custom electronic hardware for feedback and control.

3.1 System Overview

While the system described in this chapter is to be deployed from Virginia Tech's autonomous Yamaha RMAX, it was designed with the goals of being both modular and platform independent. This tethered payload deployment system is enclosed in an interchangeable payload pod, which attaches to the landing gear of the RMAX. The system has a fully capable internal processor, and can be controlled using a common RS-232 interface or conduct a mission autonomously. The system can be equipped on any aerial platform with an appropriate communications link. Some additional functionality of the internal processor is pinned out and supported, giving the system expandability.

Figure 3.1 provides an understanding of how the active electrical and mechanical components of this system interact. The System Control Unit (SCU) is the central point of communication, and receives commands from a ground-based Operator Control Unit (OCU). The System Control Unit commands the ELMO Whistle, an off-the-shelf motor controller. Additionally, the SCU receives line tension feedback and sends movement commands to the Robot Control Unit (RCU). The following sections describe these components individually.

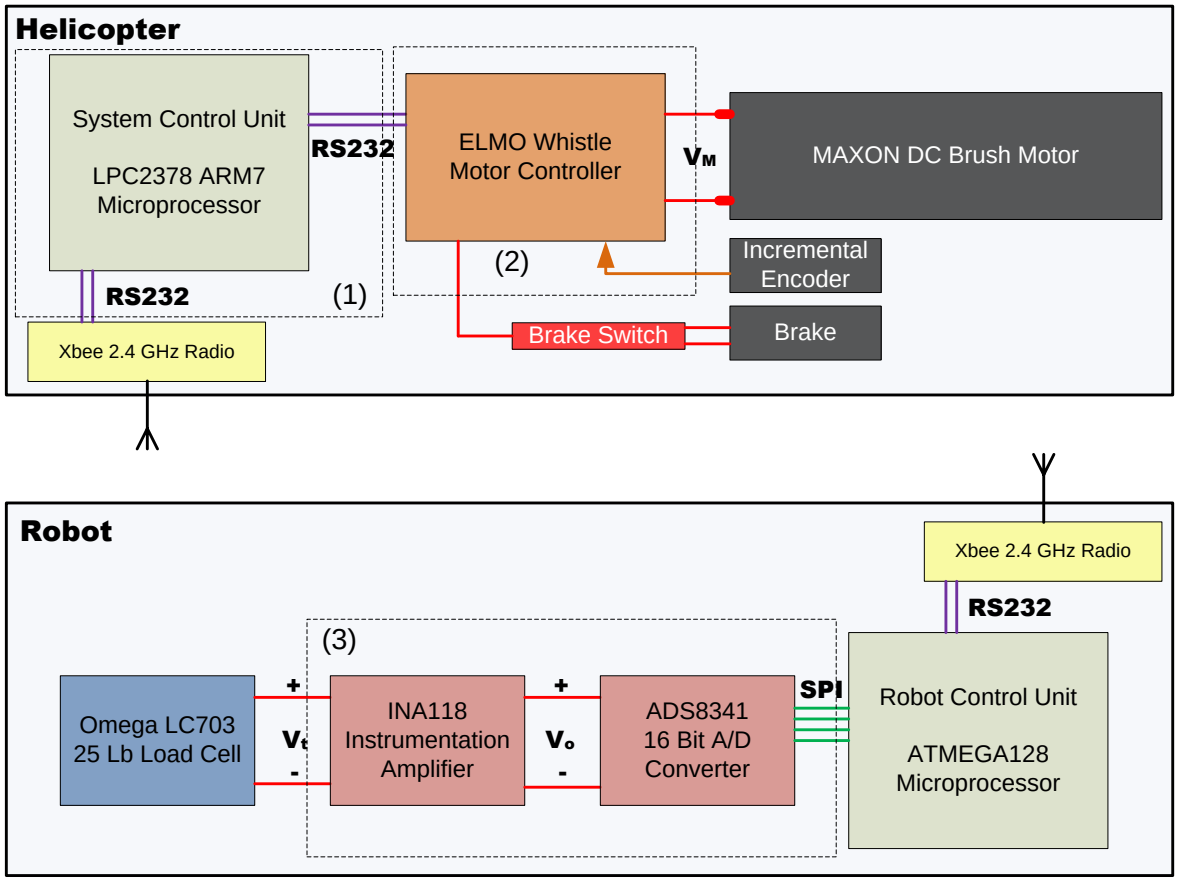

Figure 3.1: Tethered robot deployment system schematic.

3.2 Electromechanical Analysis

This section summarizes the design of the electromechanical components of the tethered payload deployment system. This consists of the winch motor and gearbox, reel and tether apparatus, and tether emergency release mechanism.

3.2.1 Electromechanical Design Requirements

The electromechanical component of this system consists of a DC Brushed Servomotor, a planetary gearhead, and an electromagnetic brake. The output shaft of the gearhead directly drives an aluminum spool of diameter 2.54 cm. This spool controls the amount of braided Spectra tether let out from the pod.

The tether suspends an 8 kg (max weight) ground robot. The minimum desired top linear speed of this robot is 0.25 m/s. Based on these criterion, the drive train requirements seen in Table 3.1 are calculated.

Table 3.1: Electromechanical Drive Train Requirements at Spool.

Spec	Value	Units
Continuous Torque Load	0.997	Nm
Braking Torque	2.0	Nm
Speed @ Torque Load	200	rpm
Power	91	W

3.2.2 Motor and Gearbox Selection

The Maxon RE40 DC brushed servomotor with a 23:1 reduction (GP42 Planetary Gear) meets the performance requirements. The manufacturer's advertised specifications [12] are given in Table 3.2.

Table 3.2: Maxon RE40 Motor Specifications.

Spec	Units	Motor	23:1 Gearing
Power Rating	W	150	
Voltage	V	24	
Inertia	gcm^2	138	252
Torque Constant	mNm/A	30.2	
Speed Constant	rpm/V	317	
No load speed	rpm	7580	330
Max Speed	rpm	12000	522
Max Continuous Torque	mNm	170	3910

This solution was simulated using MATLAB Simscape Physical Modeling toolkit to verify performance. Figure 3.2 shows the drive train's response to a 24V input at full mechanical loading. Note that the system performance of 0.45 m/s exceeds the minimum requirement. The simulated motor response is consistent with the advertised specifications.

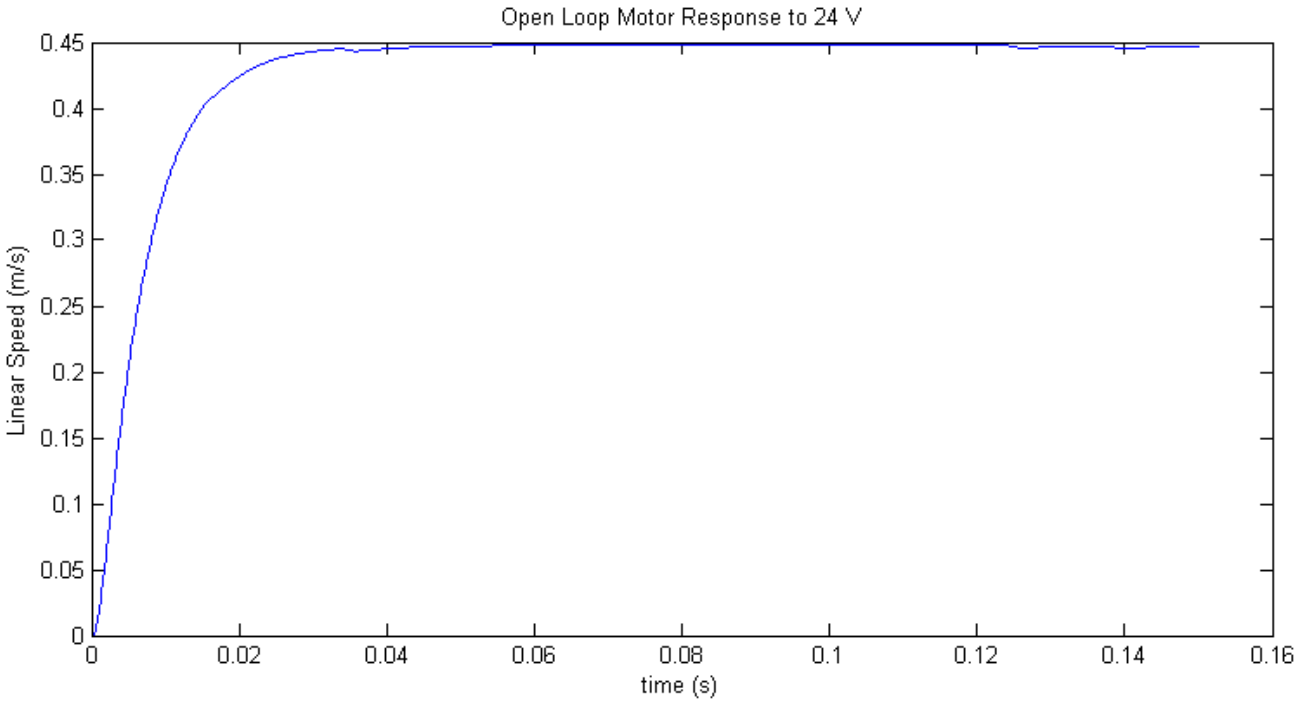

Figure 3.2: Simulated open loop drive train response under load.

3.3 Electrical Design

This section describes the key electrical design components of the tethered robot deployment system. Primary considerations in the electrical design of this system are power supply and regulation, motor control hardware, system control hardware, and system feedback hardware.

3.3.1 Power Supply and Regulation

The Tethered Payload Deployment System requires a 24 volt power supply with sufficient capacity to carry out a 45 minute mission. The power requirements for this mission are

defined below.

Table 3.3: Estimated Mission Power Demands

Mode	Power (W)	Duration (min)
Brake Engaged	5	20
Deploy/ Hoist	130	5
Tension Control	12	20
Total Draw at 22.2 V (mAh)		743

The TP3300-7SPL2, a 7 cell lithium polymer battery from ThunderPowerRC will be used. Lithium polymer batteries have a nominal voltage of 3.7 $V/cell$, and a maximum voltage of 4.2 $V/cell$ for an operating range of 25.9 - 29.4 V. The Battery has a capacity of 3300 mAh, providing a wide safety factor for a single mission. Lithium polymer batteries boast high power densities, and this cell configuration weighs only 543 g.

Provisions for a redundant power supply have been provided. This is accomplished with a Schottky diode OR-ing circuit, which will select the higher voltage and draw from it. Figure 3.3 shows the simple diode configuration. Additionally, low dropout voltage regulators provide 12 V, 5 V, and 3.3 V to various components within the pod.

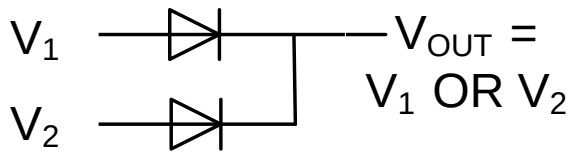

Figure 3.3: Simple Schottky diode OR-ing circuit for redundant power supply.

3.3.2 System Control Unit

The System Control Unit is a custom designed PCB which communicates with the OCU and controls all onboard hardware. At the core is an NXP LPC2378 ARM 7 microprocessor which runs an embedded version of National Instruments LabVIEW. This controller was selected due to its compatibility with LabVIEW, number of available UARTs (4), available CAN channels (2), and high flash memory (512 kB). Much of the circuitry implemented on this board was found on an open source [13] breakout board schematic for the LPC2378. This assisted greatly with the design, and allowed for a working product to be manufactured on the first design iteration.

The System Control Unit was designed for expandability, as it features pinned out and supported connectors for the following peripherals:

1. Ethernet Port
2. PWM channels for servo-actuated tether release mechanism
3. 8 Analog to Digital Converters
4. 8 General Purpose Digital I/O pins

The System Control Unit, shown in Figure 3.4, stacks with the pod's power distribution board to reduce wiring. In future iterations of this system design, it is advisable that all electronics enclosed in the pod should interface this way to reduce failure modes and save

weight and space aboard the pod.

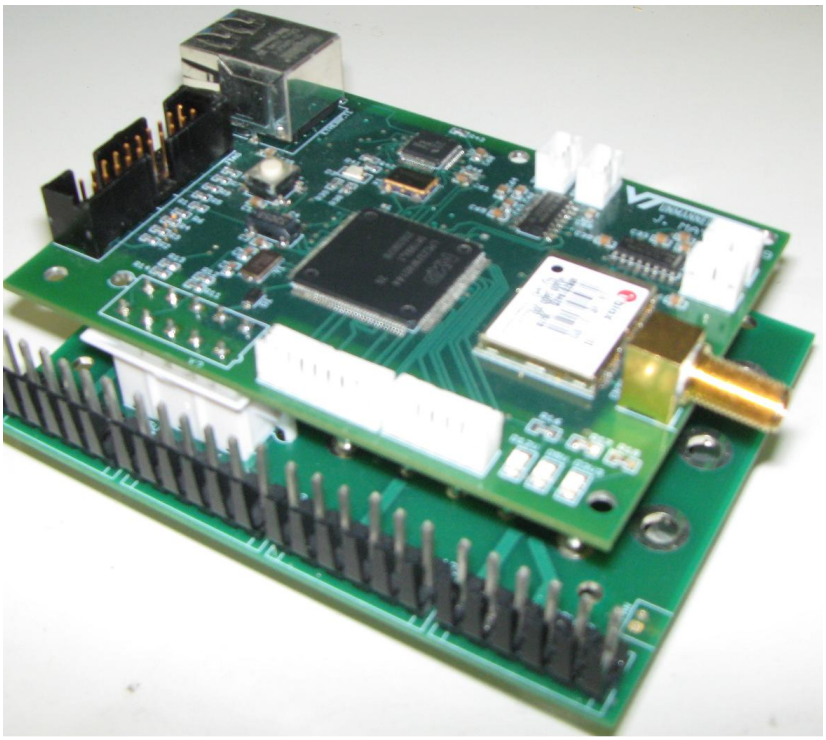

Figure 3.4: System Control Unit (SCU) stacked with Power Distribution PCB.

3.3.3 Motor Controller

The Elmo Whistle [14] is an off the shelf motor controller which executes the low level control of the winch. The Whistle features tunable position, velocity, and current loops, and receives reference commands via RS232. The tension and sway control algorithms described in the later chapters produce position or velocity reference commands for each iteration of high-level control. The Whistle will execute this command, and provide interpreted feedback from the incremental encoder.

Figure 3.5: Elmo Whistle motor controller.

When tuning the motor controller, two requirements were considered. The motor must settle at a reference position or velocity before recieving another command, and the acceleration and deceleration must be limited to avoid jerk, which may add unwanted disturbance to the system. Note that the position and velocity loops are independent, and are not simultaneously commanded. The motor controller is either in position control mode or velocity control mode. Two high level controllers are introduced later in this thesis. These high level controllers command the Elmo Whistle motor controller via reference commands. The tension controller introduced in Chapter 5 commands the position loop of the Elmo Whistle at 10 Hz, so a settling time of 0.1 s position controller is desired. The sway controller discussed in Chapter 6 commands the Speed control loop on the Whistle at 50 Hz, so a settling time

of 0.2 s is desired. Elmo's Composer software is used to tune the control gains in order to achieve this performance.

3.3.4 Tension Feedback Circuitry

Tether tension feedback is supplied by an Omega LC103 0-25 lb load cell. The load cell is mounted in line with the tether just above the ground robot mounting point, as shown in Figure 3.6. The sensor is connected to the Load Cell Instrumentation Board, which is hard mounted to the robot. The board provides 10V to the load cell, filters and amplifies the analog output signal, and converts the amplified output to a digital message when prompted by a serial device.

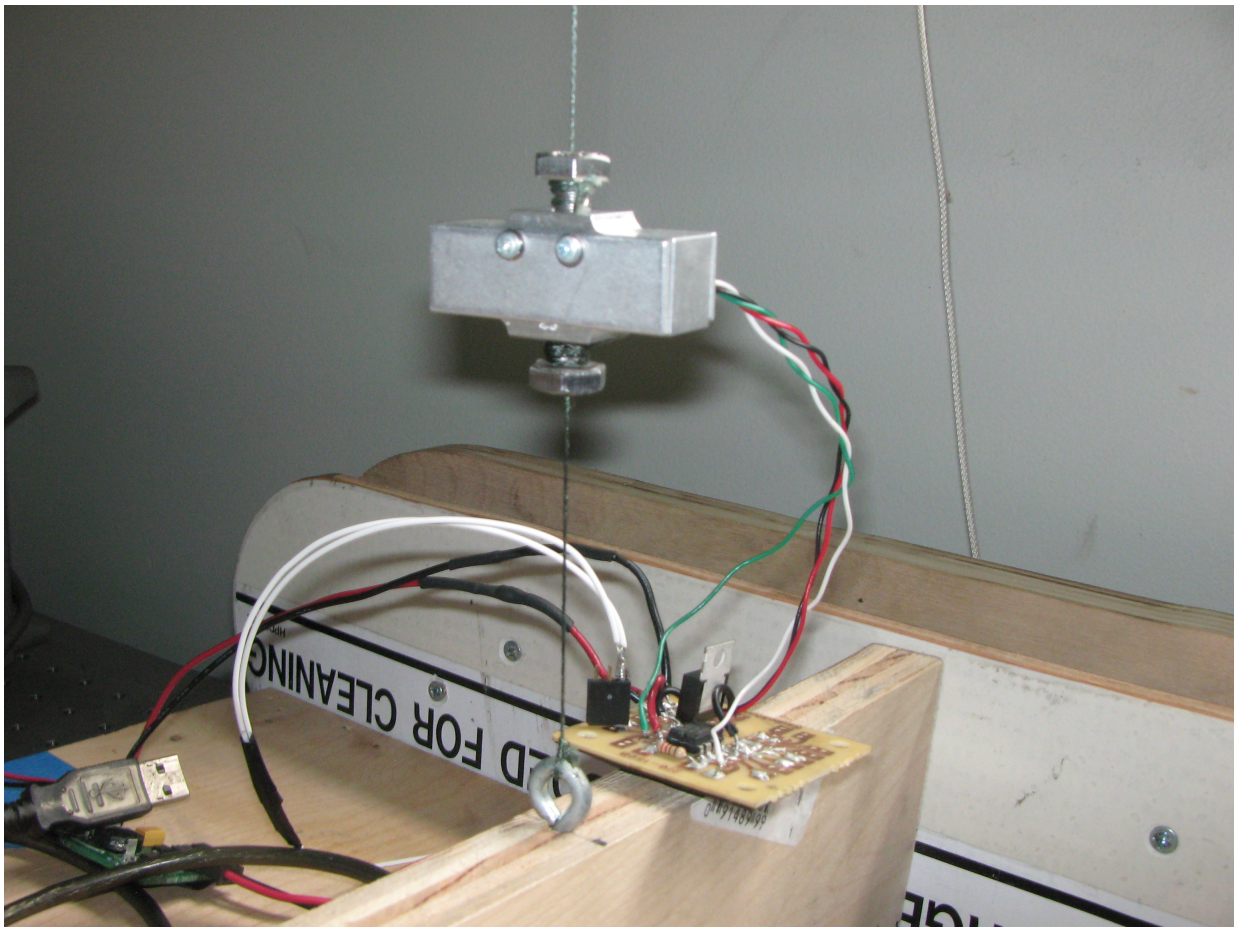

Figure 3.6: Mounting of Omega LC103 Load Cell

The full scale output of the LC103 is 2 mv/V. With a 10 V supply, the sensor will output 20 mV at full scale. To utilize the full resolution of the ADS8341 analog to digital converter chip, an instrumentation amplifier is used. The INA 118 is an adjustable instrumentation amplifier, where the gain is set by adjusting the value of an external resistor. A gain of 200 gives a full scale output of 4V. The Load Cell Instrumentation Board, shown in 3.7, packages this instrumentation circuitry, along with low drop out voltage regulators providing clean 5V and 10V power. Additionally, an optional capacitor between the high and low signal lines

can be used as a low pass filter. The output resistance of the LC103 is 350 ohm, so a single pole low pass RC filter can be added with the optional capacitor. The cut off frequency of this filter will be determined by the value of the capacitor. The board measures only 2 in. x 0.55 in. .

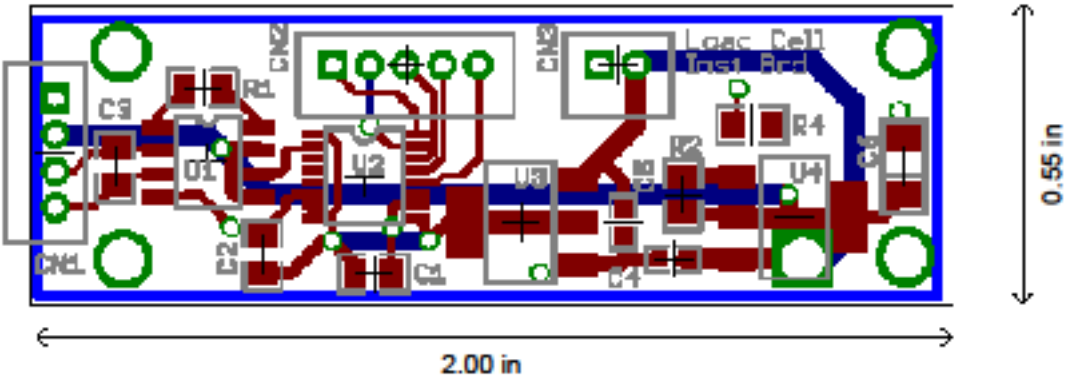

Cell Instr Brd.png

Figure 3.7: Control architecture for MATLAB simulation

The Load Cell Instrumentation Board connects with a robot controller board via Serial Peripheral Interface (SPI). Each time the robot controller board requests a reading, the Load Cell Instrumentation Board acquires a sample and reports it. The high sampling rate of the ADS8341 allows for up to 100 K samples/s. Currently, an Arduino Duemilanove serves as a prototype robot control board. Each time a sample is received, it is relayed to a controller onboard the winch pod via a 2.4GHz data link. More detail on sampling rates will be provided in the control architecture diagrams in the next chapter.

3.4 Future Design Considerations

The design of future iterations of this system should focus on adding safety functionality. Before this system is deployed on an unmanned aerial vehicle, several levels of safety and emergency modes should be in place. A tether release mechanism is needed if unexpected payload behavior or failure of the hardware occurs. This will prevent catastrophic failure of the RMAX platform. This mechanism should have built in redundancy, to insure against all modes of failure.

Another consideration for future designs is to build a tether tension apparatus on the winch pod. This will eliminate the need for wireless tension feedback, which reduces the risk of failure. Also, moving the sensor to the pod will reduce the amount of noise that is a product of the current configuration. Tether tension feedback can be accomplished by guiding the tether through a series of pullies and measuring the tensile force of one pulley, or mounting a load cell within the load path of the winch.

Chapter 4

Control Architecture and Low-Level Control

In order to achieve the high level control algorithms discussed later in this thesis on real hardware, well tuned low-level controllers are needed. This chapter discusses the architecture by which the various feedback controllers manipulate the hardware. Additionally, tuning of the low-level controllers are demonstrated for both the simulation model and physical hardware. Low-level control, in this case, refers to the speed (PID) and position (PID) controllers of the winch motor. In the physical hardware, speed and position control is accomplished using an off the shelf motor controller which is specifically tuned for this application.

4.1 Control Architecture

For the high level tension and sway control algorithms discussed in later chapters to be effective, the winch motor must be driven by well tuned current, speed, and position controllers. These high level controllers output position and speed reference commands, which the motor controller tracks. The position and speed controllers must be responsive enough to produce the desired system behavior. The position controller will be commanded at $10Hz$ while the loop operates at $1000Hz$, and the speed controller will be commanded at $50Hz$ while the loop operates at $1000Hz$.

Figure 4.1 shows the system model and cascading control architecture for tether tension control. In simulation, motor position is controlled by a PID controller with an ideal position feedback sensor. On the physical hardware system, a PID controller is used with position feedback from an incremental encoder. The resolution of this sensor is 2000 counts per motor revolution, which after gearing gives 46000 counts per spool revolution. The tension controller commands the closed loop position controller at a lower frequency. In the physical hardware, this control loop is embedded on the LabVIEW compatible ARM7 Processor. The next chapter will cover this controller in more depth and clearly define the control variables.

Figure 4.2 shows the sway control system model. Again, a cascading architecture is present. The speed controller is a closed loop PID controller, which receives motor speed feedback from the incremental encoder. The motor speed is proportional to the tether speed, $\dot{l}$. The sway controller operates at a lower frequency, allowing ample system response time between

commands. The control algorithms and variables will be explained further in Chapter 6.

For safe and efficient deployment of the robot, a well tuned speed controller is needed. This controller was developed in simulation using MATLAB Simulink and Simscape physical modeling toolbox. The controller was then verified on the physical hardware using the Elmo Whistle. A discrete time derivative of the incremental encoder output is used for the speed feedback loop. In the simulations, an ideal rotor speed sensor is used for simplicity.

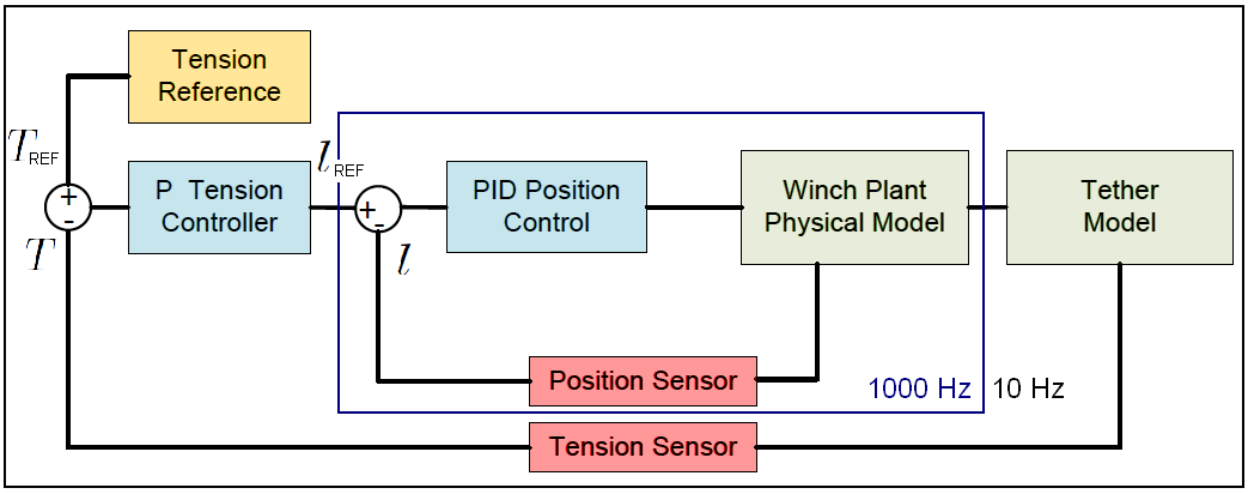

(a) MATLAB Simulink Simulation

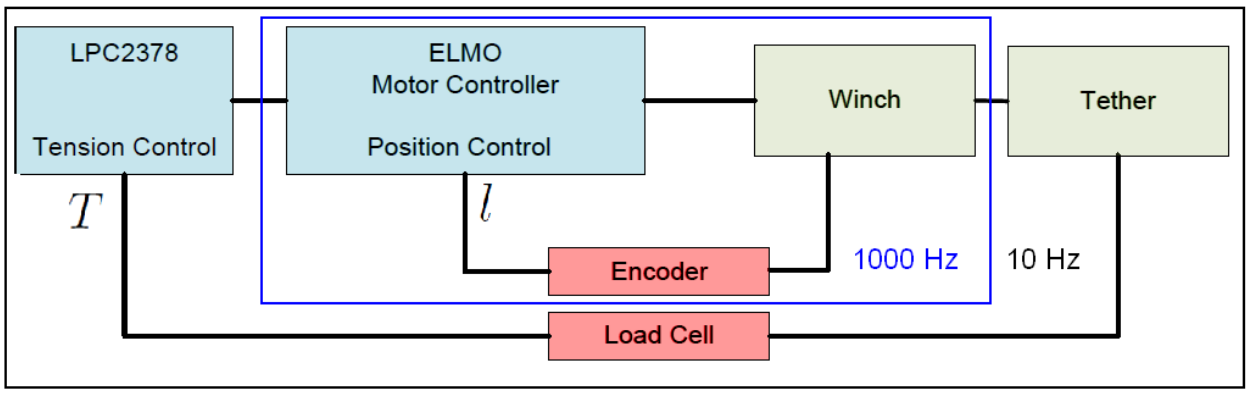

(b) Actual Hardware Setup

Figure 4.1: Tension Control Architecture

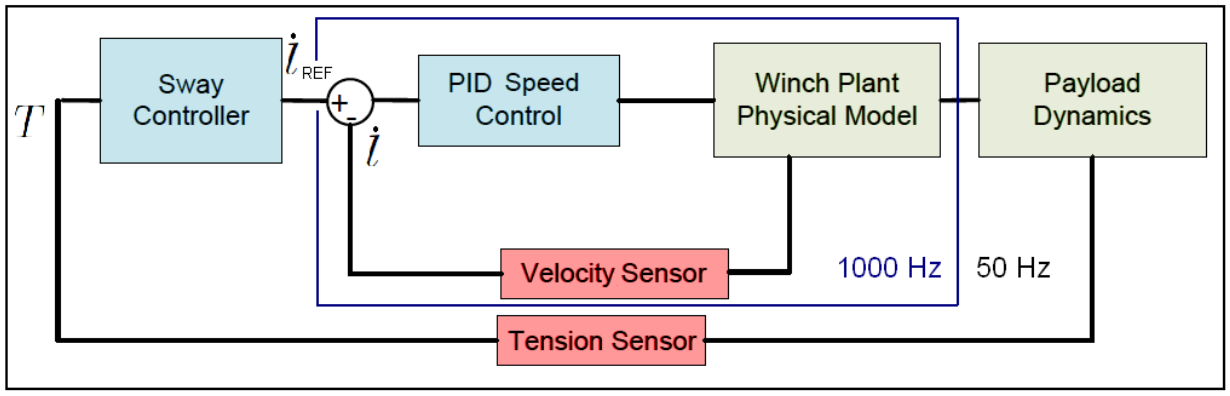

(a) MATLAB Simulink Simulation

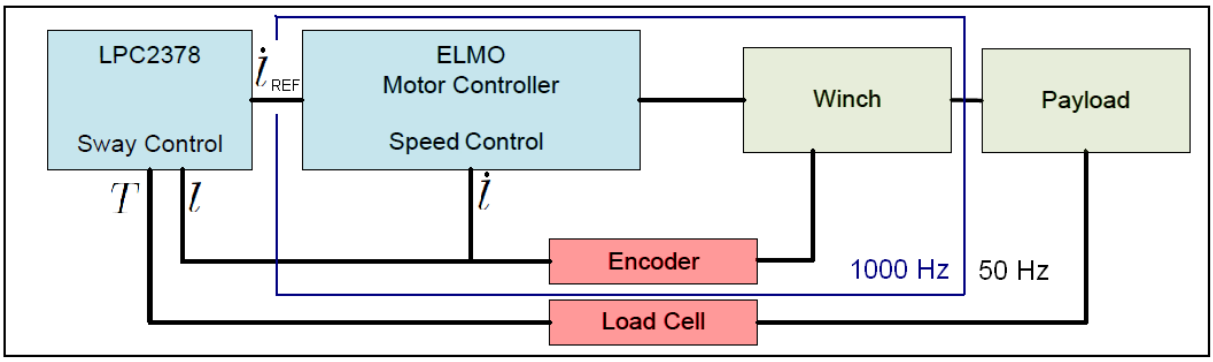

(b) Actual Hardware Setup

Figure 4.2: Payload Sway Damping Control Architecture

4.2 Position Control

It is important to know the limitations of the low level controllers so that they can be safely and properly used. The low-level position control loop must be responsive enough to reach a steady-state response within one sample of the $10Hz$ high-level tension control sample rate. To evaluate whether the position controller can meet this requirement, the following steps are taken:

1. Tune the hardware position control loop and measure system response. Tuning is accomplished by an automated process within the ELMO Composer software.

2. Build and tune a simulated controller to emulate response characteristics of the hardware controller.

3. Perform a system identification on the input-output data of the simulated response in order to obtain closed loop model.

4. Produce frequency response plots of closed loop system and identify the bandwidth.

First, the hardware controller is tuned. Figure 4.3 shows the response (blue) to a reference input (red) of $1.4cm$ calculated at the spool output. This linear distance translates to 4 revolutions of the motor. From the step response, the peak value, P_p, time at peak value, t_p, and steady state value, P_{ss} are measured. These metrics are recorded in Table 4.1.

Table 4.1: Hardware Position Controller Parameters

Metric	Value
T_{peak}	0.0442 (s)
P_{peak}	0.0143 $(counts)$
P_{ss}	0.0141 $(counts)$
$P.O.$	1.4 $percent$

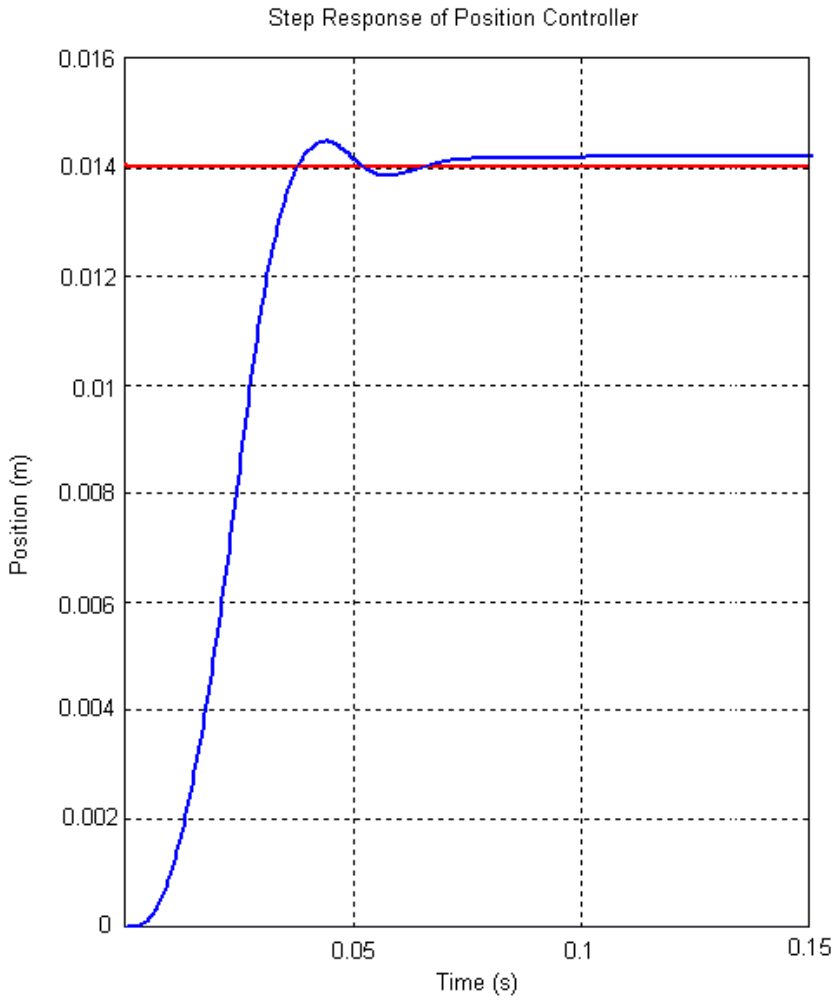

Figure 4.3: Step response of hardware position controller.

Next, a simulated position controller is designed. The controller outputs two voltages: a reference voltage for the PWM signal and a high/low voltage signal for directional control. The winch plant is simulated using MATLAB Simscape physical modeling toolkit. A screen-shot of the model and controller is shown in Figure 4.4. Simscape uses a combination of dataflow programming language and physical connections, such as electrical connections, to accurately model a hardware system.

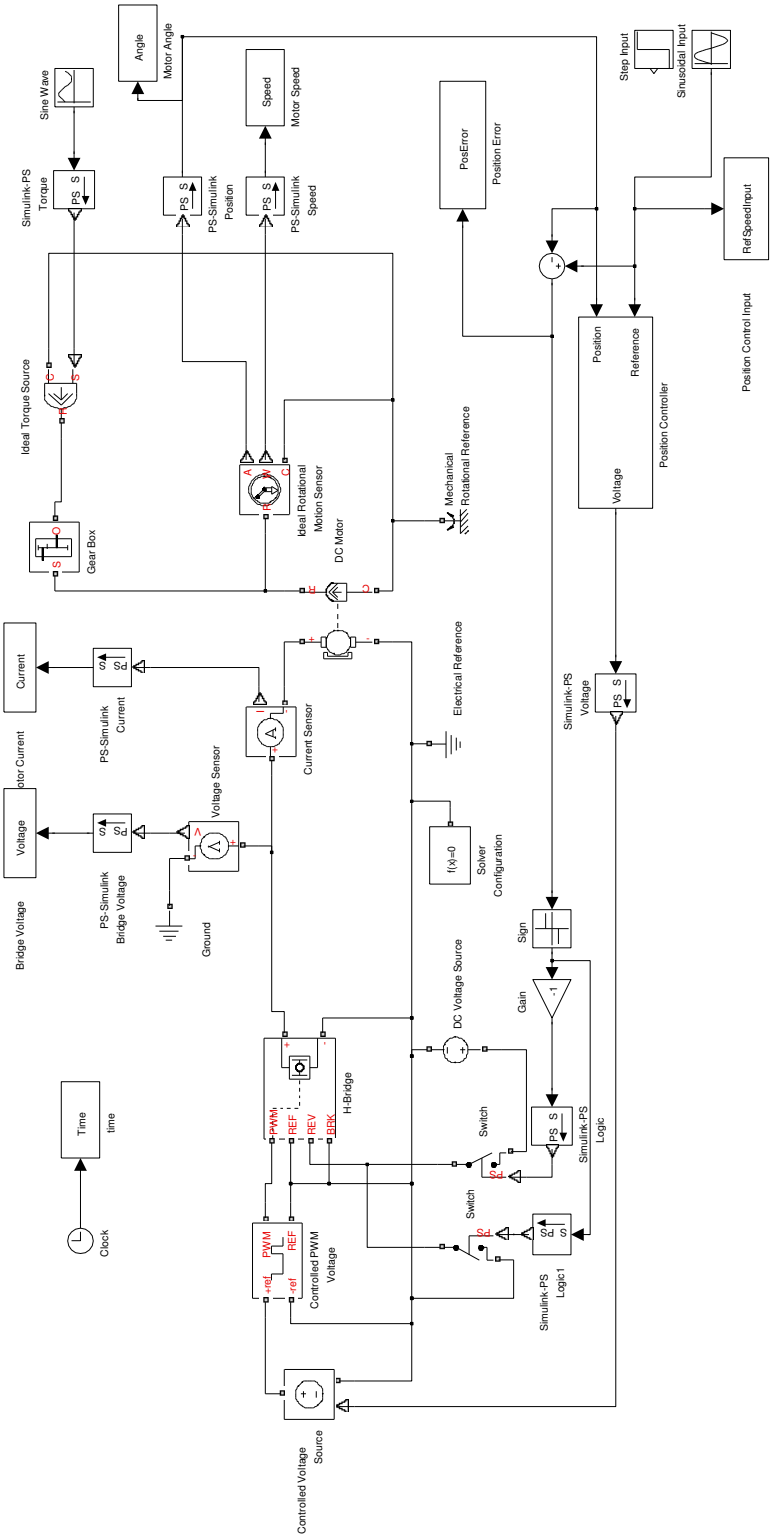

Figure 4.4: Simulink Model of Position Control and Physical Model of Plant.

This controller is tuned to have approximately the same performance characteristics as the hardware system. Figure 4.5 shows the step response of the simulated position controller. Because the ultimate goal is for the hardware controller to be capable of handling the demands of the higher leverl controller, a conservative approximation is acceptable for the simulated controller. The closed loop performance characteristics of the simulated controller are given in Table 4.2.

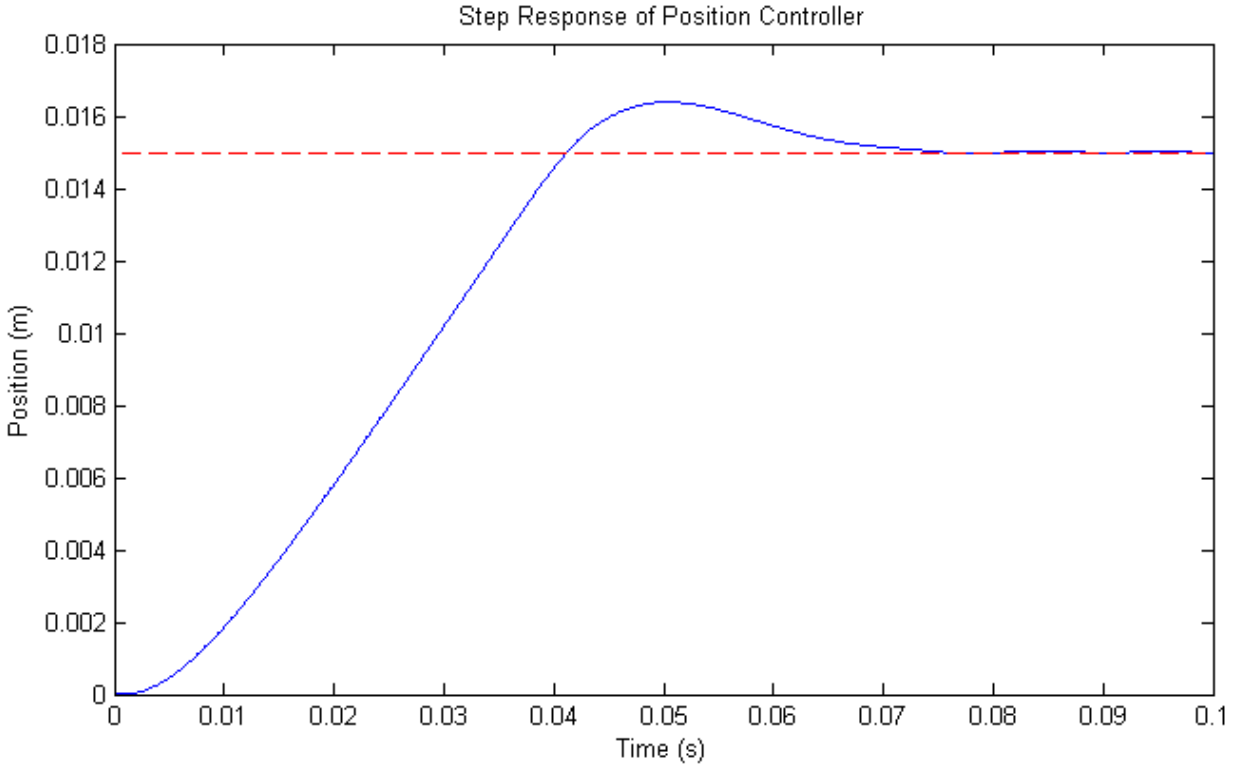

Figure 4.5: Step response of simulated position controller.

Table 4.2: Simulated Position Controller Parameters

Metric	Value
T_{peak}	0.0506 (s)
P_{peak}	0.0164 (m)
P_{ss}	0.015 (m)
$P.O.$	8.0 $percent$

Next, the system identification is performed on the closed loop response input-output data. The system identification is required because the more complex physical system model is used. This is conducted using MATLAB's System Identification toolkit. The input-output data from the step response simulation is used. Figure 4.6 shows the Bode Diagram of the estimated closed loop model from the simulated controller. The closed loop bandwidth exceeds the $62.8 rad/sec$ threshold requirement of the tension controller.

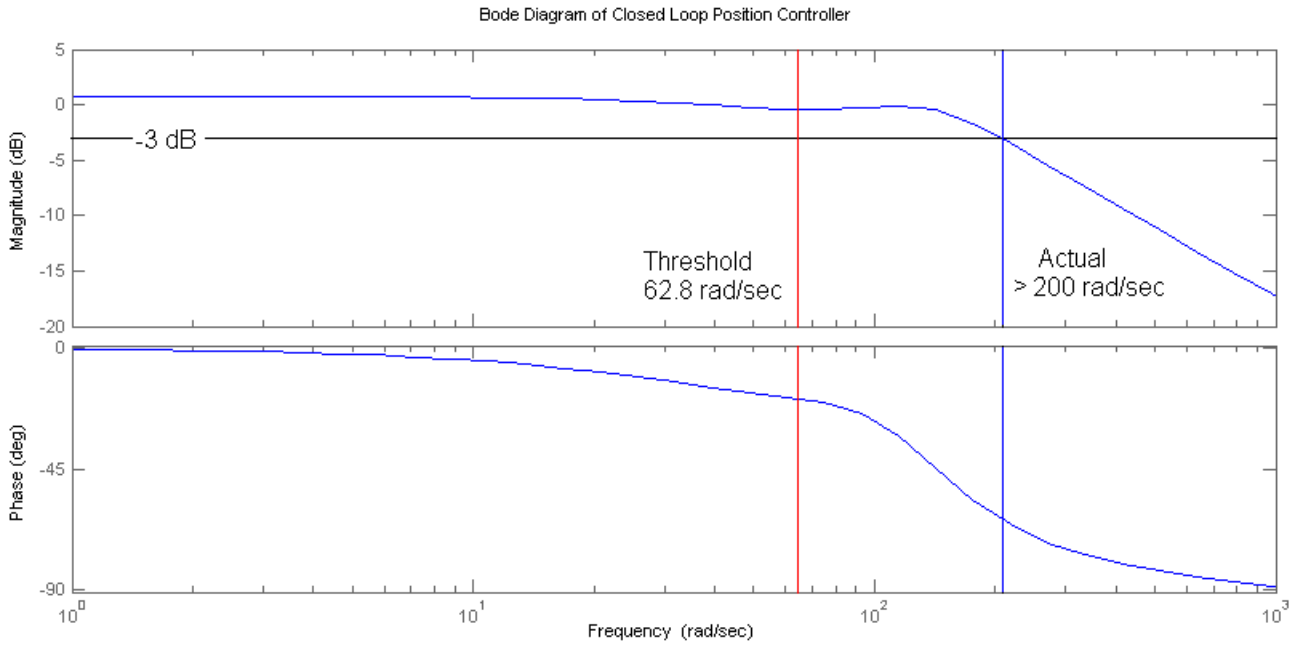

Figure 4.6: Estimated frequency response of simulated position controller.

4.3 Speed Control

Similarly, the low-level speed controller is required for high level sway control. The same steps are taken to ensure that the speed controller reaches a steady-state response within one

sample of the $50Hz$ high-level sway controller sampling rate. Again, the hardware controller is tuned and its response to a step input is evaluated. Figure 4.7 shows the experimental step response. The performance characteristics were observed and appear in Table 4.3

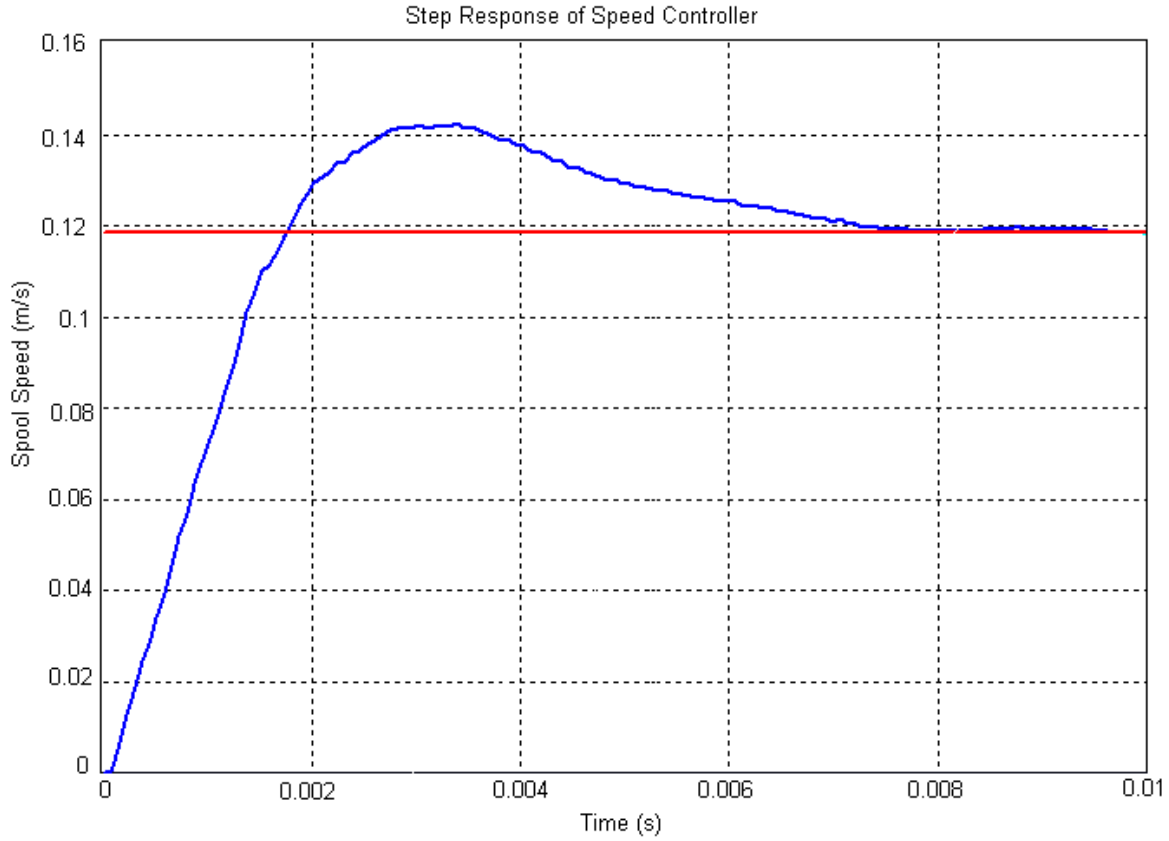

Figure 4.7: Step response of hardware speed controller.

Table 4.3: Hardware Speed Controller Parameters

Metric	Value
T_{peak}	0.0037 (s)
S_{peak}	0.142 (m/s)
S_{ss}	0.118 (m/s)
$P.O.$	20.3 *percent*

The simulated controller was modified for speed control. Figure 4.8 shows a screenshot of

the Simscape model. Again, the motor is controlled by commanding a PWM signal and direction logic value. Figure 4.9 shows the closed loop step response to a constant speed command. As shown in Table 4.4, the simulated controller is conservative with a slower peak time than the hardware model.

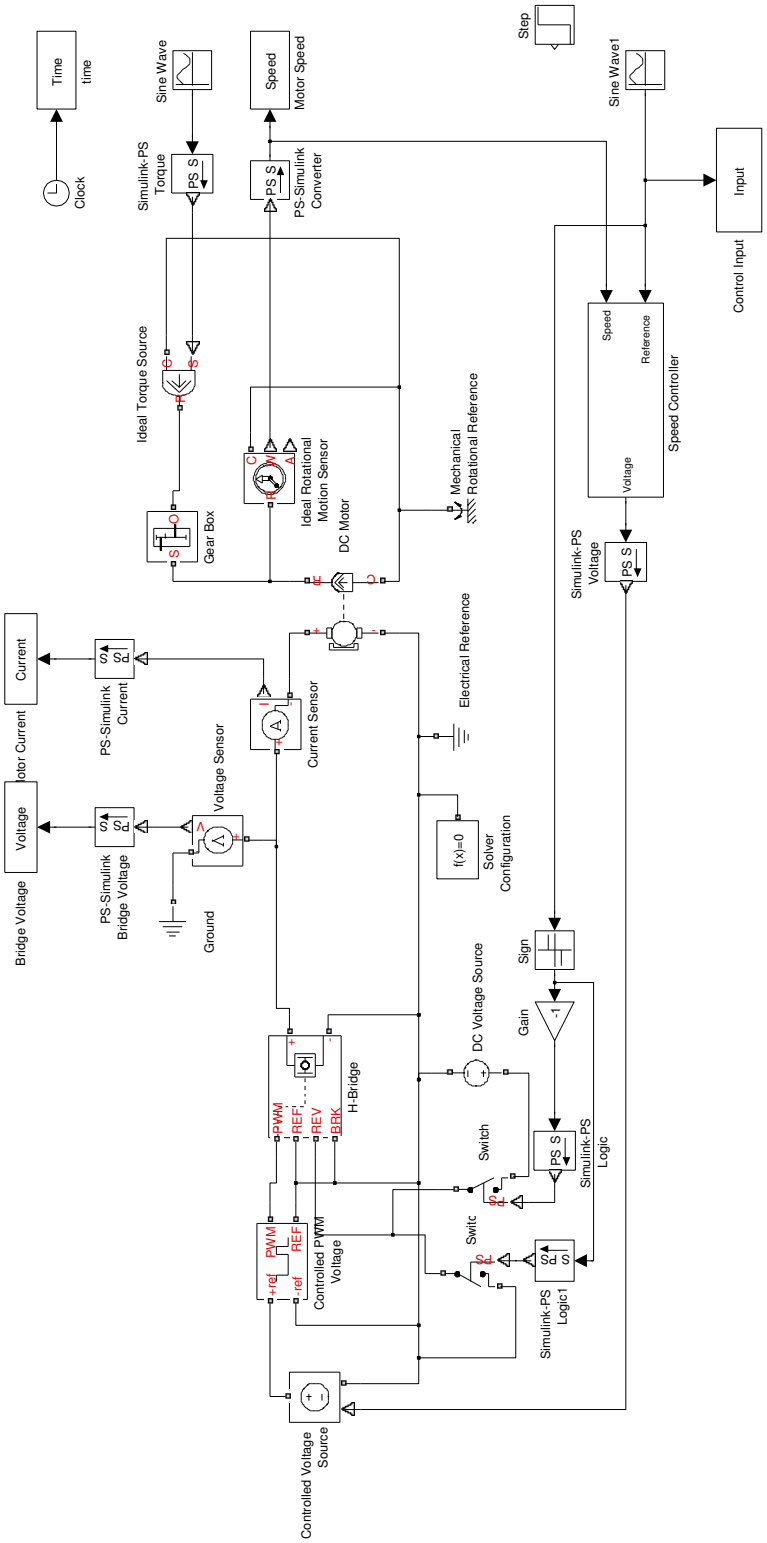

Figure 4.8: Simulink Model of Speed Control and Physical Model of Plant.

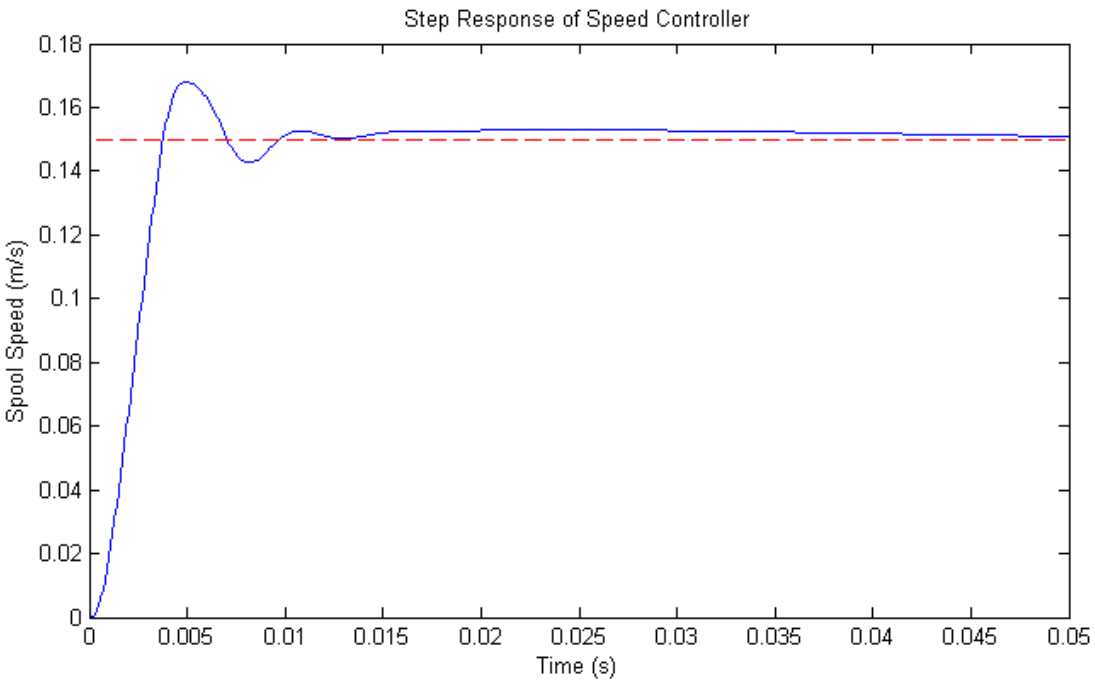

Figure 4.9: Step response of simulated speed controller.

Table 4.4: Simulated Speed Controller Parameters

Metric	Value
T_{peak}	0.0049 (s)
S_{peak}	0.169 (m/s)
S_{ss}	0.153 (m)
$P.O.$	10.4 *percent*

The frequency response of this closed loop estimation is shown in Figure 4.10. The closed loop bandwidth comfortably exceeds the threshold design requirement of $314 rad/sec$.

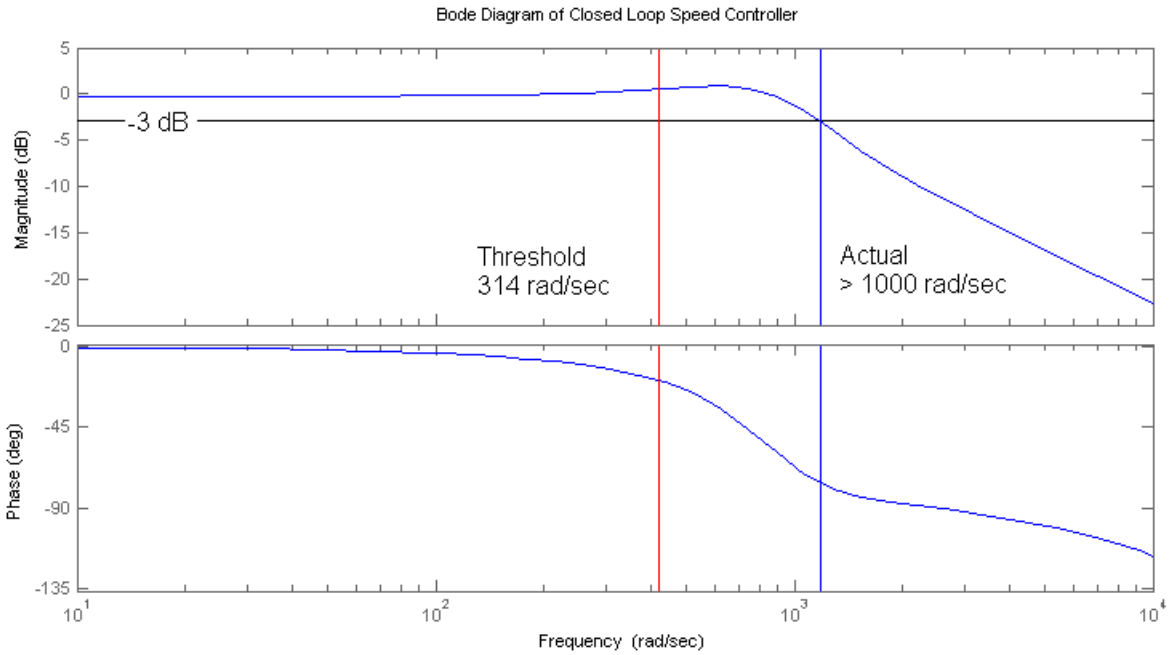

Figure 4.10: Estimated frequency response of position controllers.

Chapter 5

Tether Tension Control

During ground sampling operations, movement by the robot or the helicopter at a given tether length can either induce slack in the tether or cause the robot to be lifted off the ground. Either of these results can have a devastating impact on the success or failure of the mission. Naturally, if the robot is suddenly lifted while attempting to localize or collect samples, the likelihood of mission success is decreased. Likewise, if excess tether becomes tangled in the moving components of the robot it may be severed, resulting in the loss of the robot. Considering these possibilities, a suitable controller will lower the robot until it contacts the ground, then maintain a safe level of tether tension. This chapter describes the design and implementation of a tether tension control algorithm.

5.1 System Model and Controller

Because the cable can only support tensile loads, a piecewise model is required to describe system behavior. Figure 5.1 shows the coordinates of this model. Let r_{HP} represent the relative distance from the helicopter to the payload on the ground. The term $d_{max}(l)$ is equal to the maximum deflection of the tether. This is dependent on the payload mass, m_P, and the unstretched length, $l = r_{HP}$. From $d_{max}(l)$, the spring constant, $k(l)$, is derived. The system behavior can be categorized by one of three scenarios: (1) the tether length is in slack, (2) the tether is in the elastic region, or (3) the tether is supporting the full weight of the payload, thereby achieving the maximum tether deflection, $d_{max}(l)$. Equation 5.1 shows the tether tension, T, for each case.

$$\begin{cases} \text{if } l > r_{HP}, T = 0 \\ \text{if } (r_{HP} - d_{max}(l)) < l \leq r_{HP}, T = k(l)d_l \\ \text{if } l <= (r_{HP} - d_{max}), T = T_{max} = m_P g \end{cases} \tag{5.1}$$

The tether used in experimentation is extremely stiff. The maximum tether deflection, d_{max}, for the $4kg$ payload was measured to be $0.44mm$ at $1m$. Equation 5.2 gives the tether spring constant, $k_{tether}(l)$, as a function of tether length.

$$k_{tether}(l) \approx \frac{89000}{l}(\frac{N/m}{m}) \tag{5.2}$$

A proportional controller is proposed to control tether tension. The system dynamics will change as the distance between the helicopter and robot varies so gain scheduling will be required. Because response time is not a key design criteria for this controller, the proportional gain is tuned for stability in both directions.

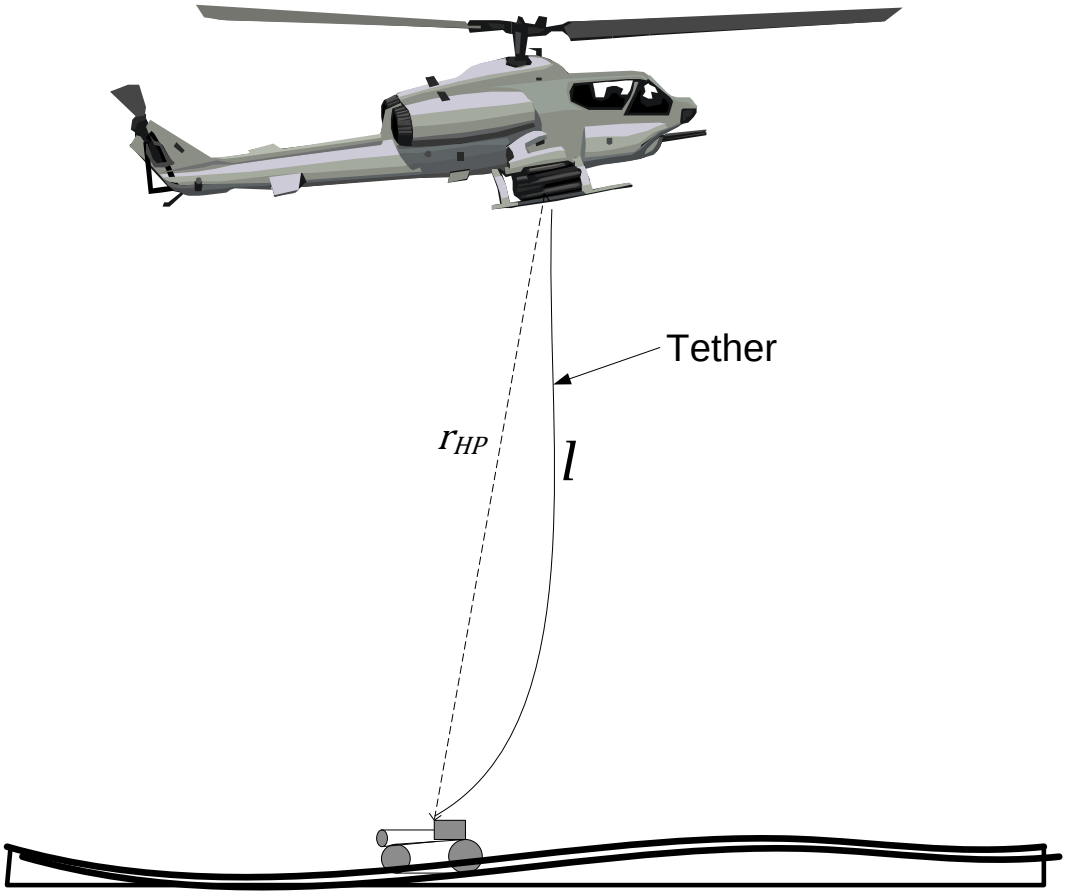

Figure 5.1: Coordinates of Helicopter-Payload System

5.2 Experimental Results

Because of the inherent discontinuity of the tether system, the tension controller must be tested for two operating conditions:

1. Lowering the robot to the ground and reaching a pre-load tension equal to a fraction of the robot weight. In this case, the pre-load tension is $3.3lb$.

2. Beginning with an initial slack in the tether, eliminate slack by applying the preload tension.

The proportional tension feedback controller is tested for each case with a unique control gain. The proportional gain is tuned by trial and error until the tension controller can approach the desired tension from either direction without instability.

For testing purposes, the robot winch pod is mounted on a cantilever attached to an electric scissor lift, emulating a hovering helicopter. This setup is shown in figure 5.2.

Figure 5.2: Experimental setup for tensioning tests

In the first test, the robot is lowered from the winch pod to the ground, and desired tension is applied. Figure 5.3 shows the sensed tether tension as the robot is lowered and reaches steady state. Although the sensor noise is significant, the tension controller remains effective. At $t = 0.65s$, the dummy robot touches down , and at $t = 0.83s$, the desired line tension is reached and maintained for the duration of the measurement.

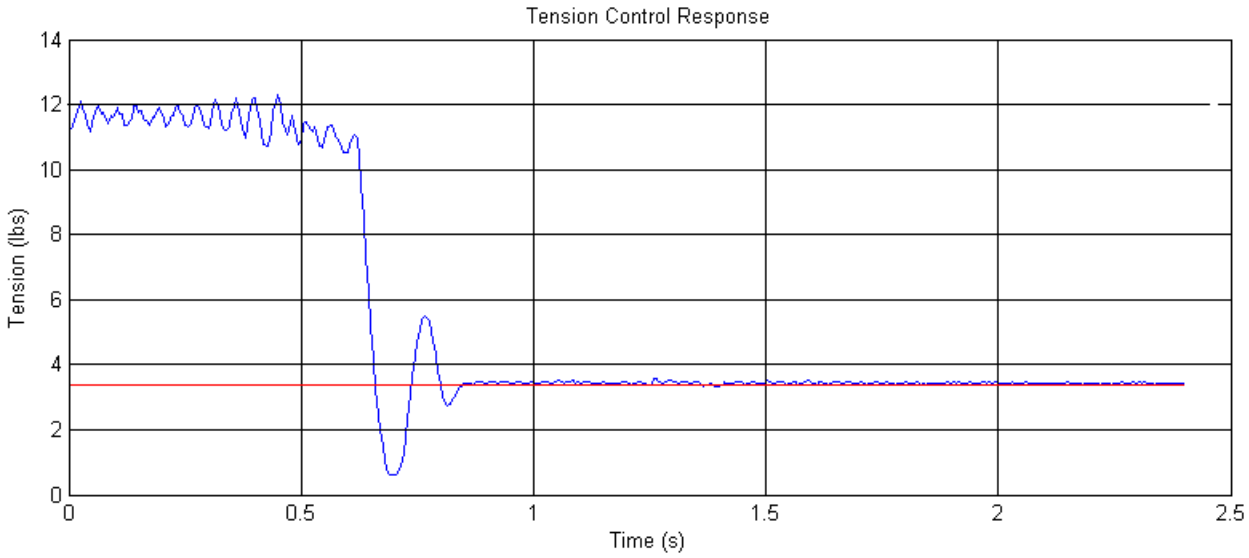

Figure 5.3: Experimental results of lowerinng and tensioning operation

The next test for this controller is to reach and maintain desired tether tension from slack initial condition. Figure 5.4 shows the system response. The load cell first senses tension at $t = 1.45s$. At 1.58, the controller reaches the steady state value. With these control gains, the controller is able to reach the desired tether tension from either direction. This meets the design criterion.

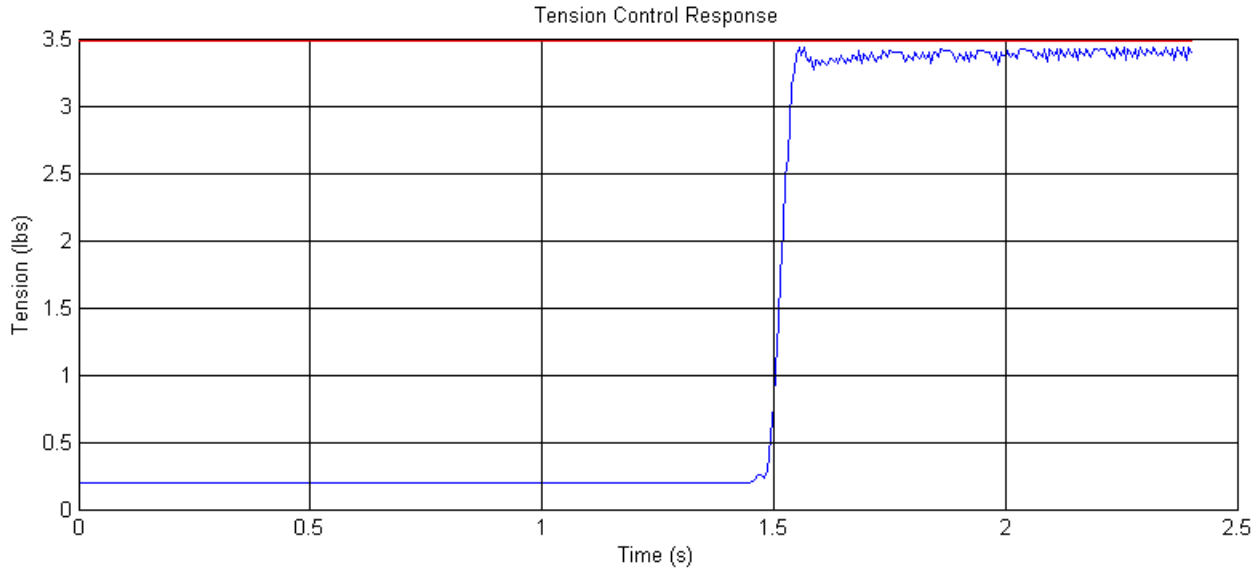

Figure 5.4: Experimental results of tensioning from slack condition

Chapter 6

Damping Control of Payload Oscillation

This chapter investigates a solution to controlling payload sway with vertical actuation. Payload sway algorithms which employ movements of the helicopter have been studied and proven effective in the literature. The intent of this work is to examine a sway control algorithm which employs only the actuation of the winch. The algorithm analyzed and tested in this chapter is effective in reducing payload sway about a desired tether length and particularly during hoist. This algorithm is a passive damping technique, which is robust to high sensor noise and system nonlinearity. Active damping techniques were not examined, though there may exist more effective methods of controlling payload sway with winch actuation.

6.1 Background Information

Potentially hazardous pendulations of the tethered payload can occur during hoisting. These pendulations, if large enough, can affect the stability of the helicopter. There has been much research conducted toward stabilizing this multibodied system. Most of these control techniques require corrective movements of the helicopter. The controller described in this chapter uses only vertical actuation of the robot to dampen sway. This is because

1. The system is to be functional independent of which UAV platform which supports it, and
2. Most helicopter flight controllers cannot control swinging payloads as tether length gets smaller.

For these reasons, the nonlinear controller introduced by [11] is an appropriate approach to sway control.

6.2 Variable Length Pendulum Dynamics

Suspending a slung load from a helicopter platform represents a very complex multi degree of freedom system. Accounting for tether configurations, aerodynamic effects, and various causes of helicopter motion can further complicate this model. However, a simple model can be used to analyze the payload dynamics and effectiveness of this controller for the reasons

listed below:

1. A single, stiff, lightweight tether is used. Because this tether is always in tension, it can be approximated as a rigid, massless rod.

2. Aerodynamic effects contribute to energy dissipation during payload sway, thus ignoring them is conservative.

3. There is no moment at the connection point of the tether and the payload. For this reason, the inertia of the payload is ignored, and the payload is modeled as a point mass.

4. The method of controlling payload sway with vertical actuation is only effective in reducing sway due to pendulation, and has no authority over rotational movement of the payload. Because of this, a two dimensional model can be used.

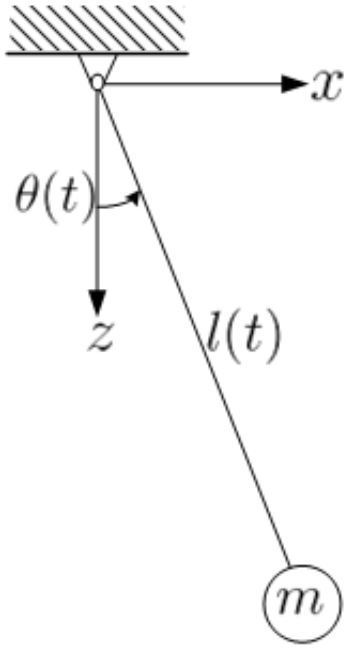

Figure 6.1: Coordinate frame of payload dynamics model

Consider the coordinate system in Figure 6.1. The payload is represented as a point mass attached to a rigid, massless rod of time-variable length. The rod is hinged on the other end to a rigid reference point. The Lagrangian method is used to derive the equations of motion.

Position and velocity equations are necessary to derive the kinetic and potential energy equations. Equation 6.1 shows the position of the point mass at time t,in terms of l and θ.

$$x(t) = l(t)sin\theta(t) \qquad z(t) = l(t)cos\theta(t) \tag{6.1}$$

Differentiating yields the velocity vectors, shown in Equation 6.2

$$\dot{x} = \dot{l}(t)sin\theta(t) + l(t)\dot{\theta}(t)cos\theta(t) \qquad \dot{z} = \dot{l}(t)cos\theta(t) - l(t)\dot{\theta}(t)sin\theta(t) \tag{6.2}$$

The resulting kinetic and potential energy of the payload are solved in Equations 6.4 and 6.6, respectively.

$$\begin{aligned} T &= \frac{1}{2}m[\dot{x}(t)^2 + \dot{z}(t)^2] && (6.3)\\ &= \frac{1}{2}m\dot{l}(t)^2[sin^2\theta(t) + cos^2\theta(t)] + \\ &\quad \frac{1}{2}m[\dot{l}l\dot{\theta}sin\theta cos\theta - \dot{l}l\dot{\theta}sin\theta cos\theta] + \\ &\quad \frac{1}{2}ml(t)^2\dot{\theta}(t)^2[sin^2\theta(t) + cos^2\theta(t)] \\ &= \frac{1}{2}m[\dot{l}(t)^2 + l(t)^2\dot{\theta}(t)^2] && (6.4) \end{aligned}$$

$$\begin{aligned} U &= -mgz(t) && (6.5)\\ &= mgl(t)cos\theta(t) && (6.6) \end{aligned}$$

The resulting Lagrangian is

$$L(\theta(t),\dot{\theta}(t)) = T - U \tag{6.7}$$

$$= \frac{1}{2}m[\dot{l}(t) + l(t)^2\dot{\theta}(t)^2] - mgl(t)cos\theta(t)$$

$$= \frac{1}{2}m[l(t)^2\dot{\theta}(t)^2 - 2gl(t)cos\theta(t) + \dot{l}(t)^2] \tag{6.8}$$

Applying Lagrange's Equation, 6.9, and solving gives the equation of motion of the time variable pendulum. This solution is given in terms of $\theta(t)$, $\dot{\theta}(t)$, $l(t)$, and $\dot{l}(t)$, in Equation 6.10.

$$0 = \frac{d}{dt}\left(\frac{\partial L}{\partial \dot{\theta}}\right) - \frac{\partial L}{\partial \theta} \tag{6.9}$$

$$= \frac{d}{dt}ml(t)^2\dot{\theta}(t) + mgl(t)sin\theta(t)$$

$$= m[l(t)^2\ddot{\theta}(t) + 2l(t)\dot{l}(t)\dot{\theta}(t)] + gl(t)sin\theta(t)$$

$$= \ddot{\theta}(t) + \frac{2\dot{l}(t)\dot{\theta}(t)}{l(t)} + \frac{gsin\theta(t)}{l(t)} \tag{6.10}$$

A model is built using simulink to demonstrate the effect of reducing tether length at a constant rate while the payload is oscillating. Figure 6.2 shows that as tether length decreases, the amplitude of oscillation increases. It is obvious that an uncontrolled hoist of an oscillating payload could have dangerous ramifications.

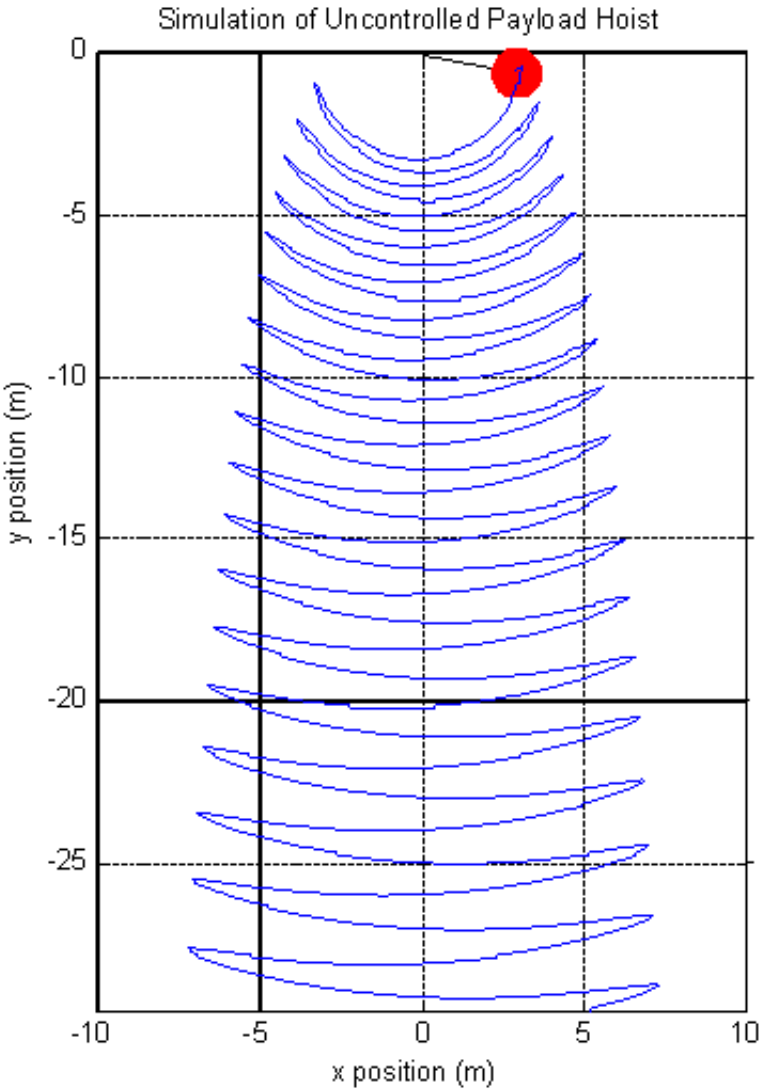

Figure 6.2: Path of tethered payload during uncontrolled hoist.

6.3 Damping by Autoparametric Resonance

This section describes an effective control approach to damping payload sway with only vertical, i.e. winch, actuation. The following pages define and derive the control structure

and analize the results of computer simulation of the system.

6.3.1 Elastic Pendulum System

A system that consists of two or more vibrating components which are coupled in a nonlinear fashion is said to be an autoparametric system [15]. Within such a system, the vibration of one component can excite vibrations in the other component. Within autoparametric systems are a primary system and one or more secondary systems. By definition, the secondary system may be at rest while the primary system is vibrating. Perhaps the most famous example of an autoparametric system is one which consists of a point mass pendulum on a massless visco-elastic tether. In this system, shown in Figure 6.3, the primary vibration mode is that of the visco-elastic tether, and the secondary mode is the oscillattion of the pendulum. This is because the pendulum motion can be zero while the tether system vibrates, but the reverse is impossible. When the excitation of the visco-elastic tether system is in 2:1 resonance with the pendulum system, energy is transferred between the two modes. This is an autoparametric resonance. Let k and d denote the stiffness and damping parameters of the visco-elastic tether, respectively.

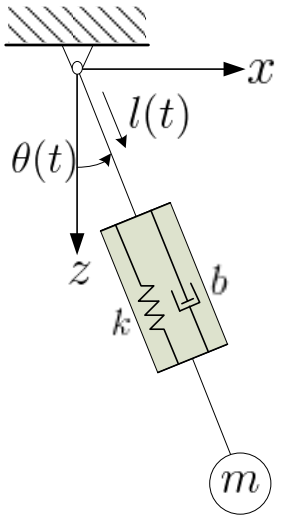

Figure 6.3: Elastic Pendulum System

The equations of motion for the elastic pendulum can be derived by coupling the dynamics of the variable length pendulum from Equation 6.10 with the SDOF visco-elastic tether. Let l_0 represent the equilibrium tether length at $\theta = 0$.

Figure 6.4 shows the forces acting on the tethered payload. F_{pend} represents the forces due to pendulum motion and F_{spring} represents the forces due to the spring-damper tether.

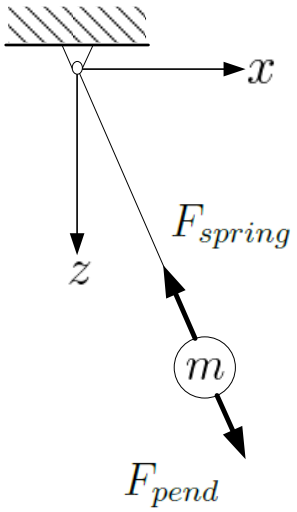

Figure 6.4: Free body diagram showing payload forces as defined in Equation 6.11.

From Newton's Second Law of Motion:

$$\begin{aligned} m\ddot{l} &= \sum F \\ &= F_{pend} - F_{spring} \\ &= m\dot{\theta}^2 l - mg(1 - cos\theta) - k(l - l_0) - b(\dot{l} - \dot{l}_0) \end{aligned} \tag{6.11}$$

$$0 = \ddot{l} - \dot{\theta}^2 l + g(1 - cos\theta) + \frac{k}{m}(l - l_0) + \frac{b}{m}(\dot{l} - \dot{l}_0) \tag{6.12}$$

Combining the result with Equation 6.10 from the previous section, the equations of motion for the elastic pendulum system are shown below. Note that the nonlinear coupling fits the

criterion for an autoparametric system.

$$0 = \ddot{\theta} + \frac{2\dot{l}\dot{\theta}}{l} + \frac{gsin\theta}{l}$$
$$0 = \ddot{l} - \dot{\theta}^2 l + g(1 - cos\theta) + \frac{k}{m}(l - l_0) + \frac{b}{m}(\dot{l} - \dot{l}_0)$$

6.3.2 Emulated Visco-Elastic Control Structure

This section describes a control strategy which relies on a small angle assumption for pendulum angle and neglects aerodynamic damping. Because these assumptions may not be valid for a real system, a second control strategy is introduced later which applies the same principles described here, but is more robust to an actual system.

In order to achieve pendulum damping of the payload, the controller will imitate the response of the visco-elastic element of the visco-elastic pendulum system described in the previous section. For this particular analysis, we will assume that the tether compliance is negligible, therefore emulation of the stiffness and damping dynamics will be obtained through modulation of the tether length, l. This controller will be tuned so that the frequency of the spring-mass-damper system is in a 2:1 resonance with the pendulum frequency. Because the pendulum frequency varies as the tether length changes, the emulated stiffness and damping parameters must adapt. To solve for these parameters, consider the response of the mass-spring-damper system when $\theta = \dot{\theta} = 0$. Let ω_n represent natural frequency, and ζ represent damping ratio.

$$\ddot{l} = -\frac{b}{m}(\dot{l} - \dot{l}_0) - \frac{k}{m}(l - l_0) \tag{6.13}$$

$$= -2\zeta\omega_n(\dot{l} - \dot{l}_0) - \omega_n^2(l - l_0) \tag{6.14}$$

Equations 6.13 and 6.14 are used to solve for the natural frequency and damping ratio:

$$\omega_n = \sqrt{\tfrac{k}{m}} \qquad\qquad \zeta = \tfrac{1}{2}\tfrac{b}{\sqrt{mk}} \tag{6.15}$$

Solving for the resonant frequency of the system:

$$\omega_r = \omega_n\sqrt{1 - 2\zeta^2} \tag{6.16}$$

$$= \sqrt{\frac{k}{m} - \frac{b^2}{2m^2}} \tag{6.17}$$

The resonant frequency of the emulated visco-elastic tether is tuned to twice the frequency of pendulation, ω_{pend}.

$$\omega_r = 2\ \omega_{pend} \tag{6.18}$$

$$\sqrt{\frac{k}{m} - \frac{b^2}{2m^2}} = \sqrt{\frac{g}{l_0}} \tag{6.19}$$

Solving for k and b, in terms of ζ and l_0:

$$k = \frac{4mg}{(1-\zeta^2)l} \qquad\qquad b = 2\sqrt{mk}\zeta \tag{6.20}$$

These parameters are adaptively varied for each control iteration. At each control iteration, the control strategy is shown below:

1. Aquire the measurements for l and $\dot{l}$.
2. Estimate ω_r from Equation 6.19.
3. Calculate k and b from Equation 6.20.
4. Calculate the resulting emulated spring forces as shown in the right hand side of Equation 6.13.
5. Apply reference to tension controller.

The damping ratio, $0 \leq \zeta \leq 1$, is tuned to yield the best results. If ζ is too low, the system will only transfer energy between vibration modes and will not achieve energy dissipation.

If ζ is too high, energy dissipation will be slow. To understand the relationship of system performance and ζ, 1000 hoists are simulated for damping ratios ranging from $0.001 \leq \zeta \leq 0.5$. The angle attenuation is the ratio of the payload angle at the peak of the final oscillation to the initial angle. For damping ratios between $0.015 \leq \zeta \leq 0.265$, at least some attenuation of the pendulum angle occurs. Damping ratios outside of this range should not be selected, as they actually increase payload angle. The optimal damping can easily be identified as the low point on this curve. This occurs at $\zeta = 0.043$.

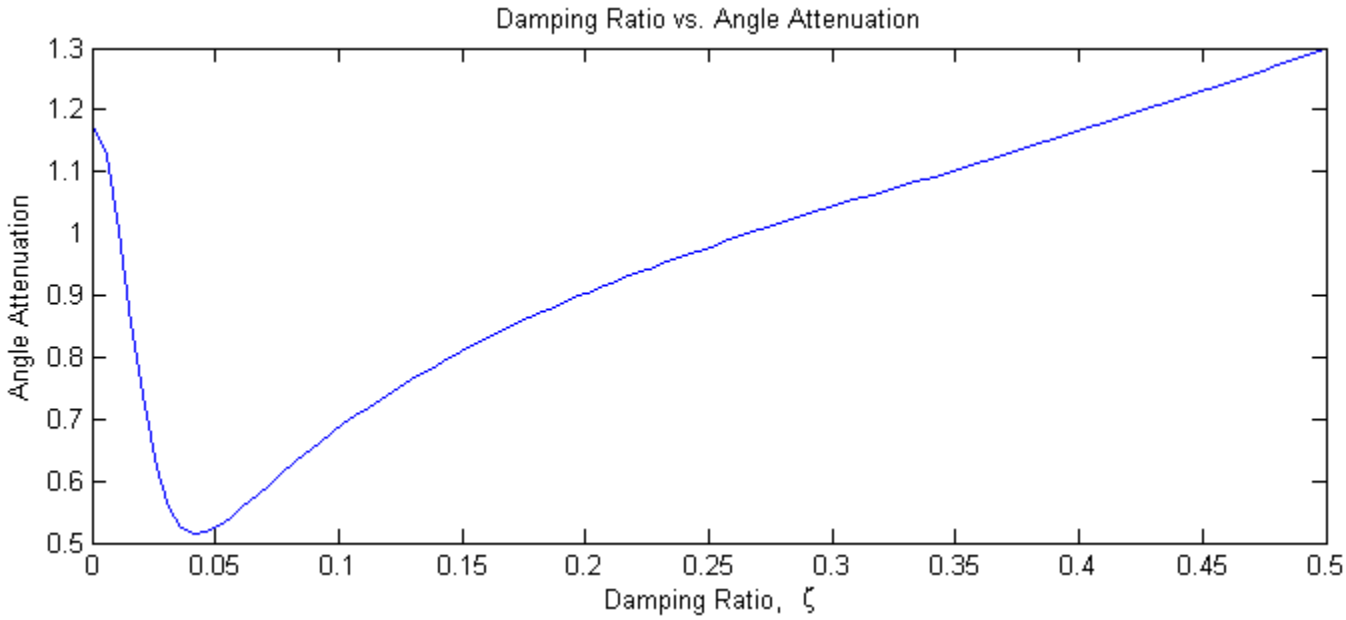

Figure 6.5: Angle Attenuation for various damping ratios.

6.3.3 Tension Feedback Control Strategy

With the emulated visco-elastic tether control structure, the resonance condition relies on the small angle approximation. Because of this, the pendulum angle of the actual payload

dynamic system will become out of phase with the pendulum angle of the reference system that the controller relies on. When the pendulum angle of the actual system and assumed angle of the controller go out of phase, the autoparametric resonance can shift from a damping phenomenon to excitation of the pendulum. To avoid this, another approach can be used. A simple proportional controller can be implemented which varies the tether length rate of change proportional to the tether tension relative to equilibrium. This ensures that the vertical control efforts are always in a natural 2:1 resonance with the pendulum angle, and is therefore more robust to large pendulation angles and aerodynamic damping. Figure 6.6 shows the winch-payload system. The winch controls the tether length by applying an appropriate torque to the spool shaft. When the tether length rate of change, $\dot{l}$, is controlled proportional to the tension relative to equilibrium, $T - T_{eq} = T - mg$, the dynamics of the pendulum are altered in such a way that reduces payload sway. For hoisting, the proportional rate length of change is superimposed on a constant rate, $\dot{l_0}$.

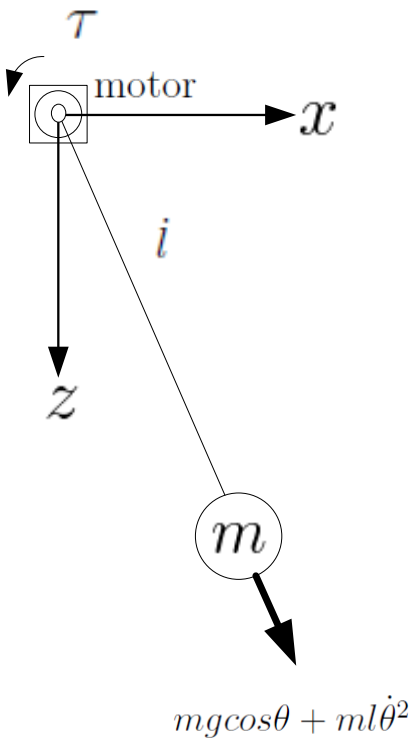

Figure 6.6: Free body diagram of winch controlled payload.

For simulation of the payload dynamics and controller, a model is built in MATLAB Simulink. The payload model is based on the nonlinear dynamics of the two dimensional variable-length pendulum derrived in this chapter. Initially, an ideal force sensor is used for feedback. Tether length for this simulation is initiated at $l_0 = 40m$. Three different initial pendulum angles are used in order to demonstrate the controller's effectiveness. Angles of $\theta_0 = 5$, $\theta_0 = 10$, and $\theta_0 = 15$ are simulated. In each case, $\dot{\theta_0} = 0 degrees/sec$ and $\dot{l_0} = 0.2$. Figure 6.7 shows the payload trajectory through a full hoist for each set of initial conditions. Note that the controller is more effective for higher initial payload angles.

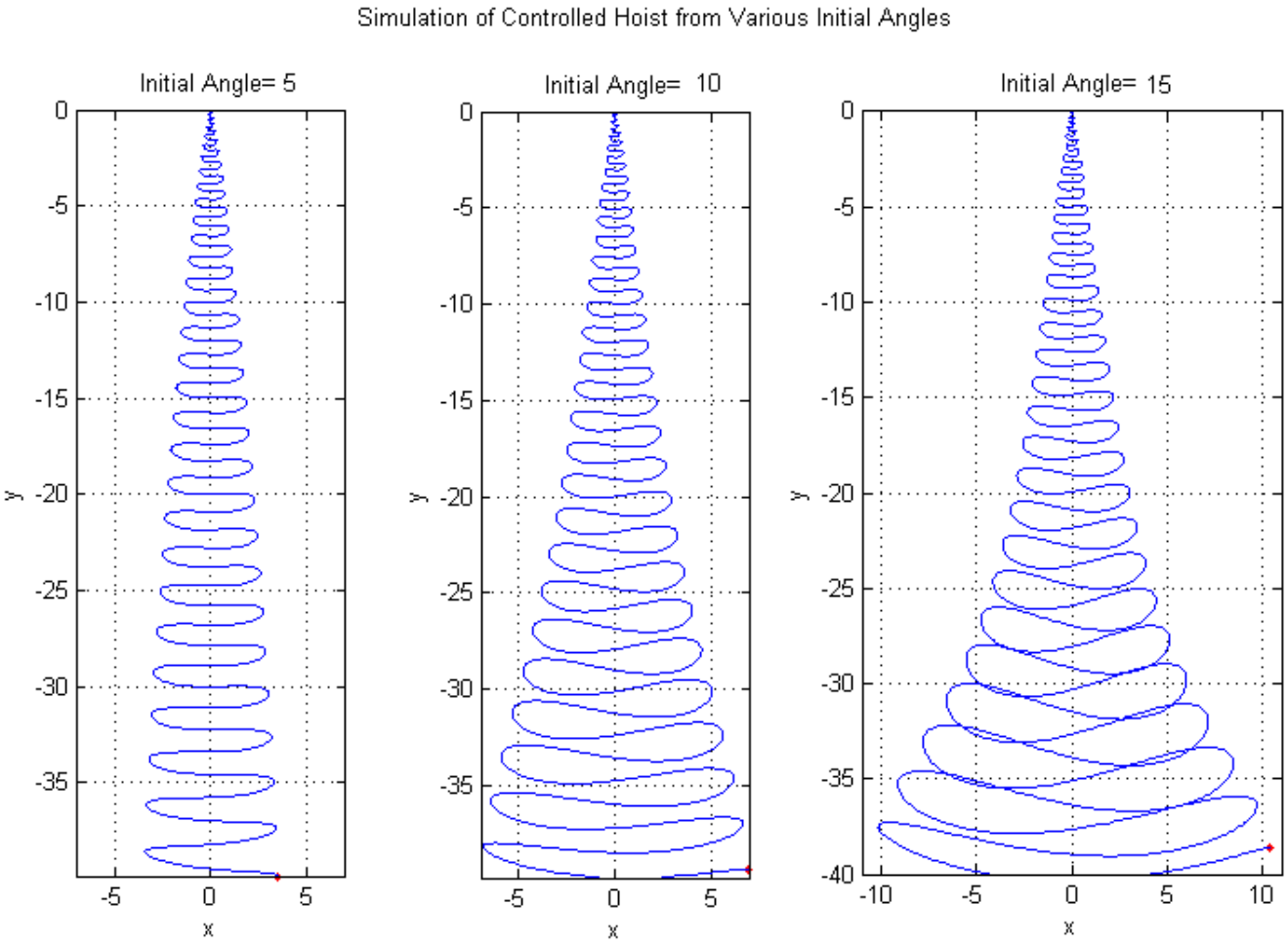

Figure 6.7: Simulation results controlled hoists.

To illustrate how the winch acts as an energy dissipater, Figure 6.8 shows $l - l_0$, $\dot{l}$, and $T - T_{eq}$ over one pendulum cycle. Notice that the tension relative to equilibrium opposes the tether speed for every point in time. This result is dissipative work.

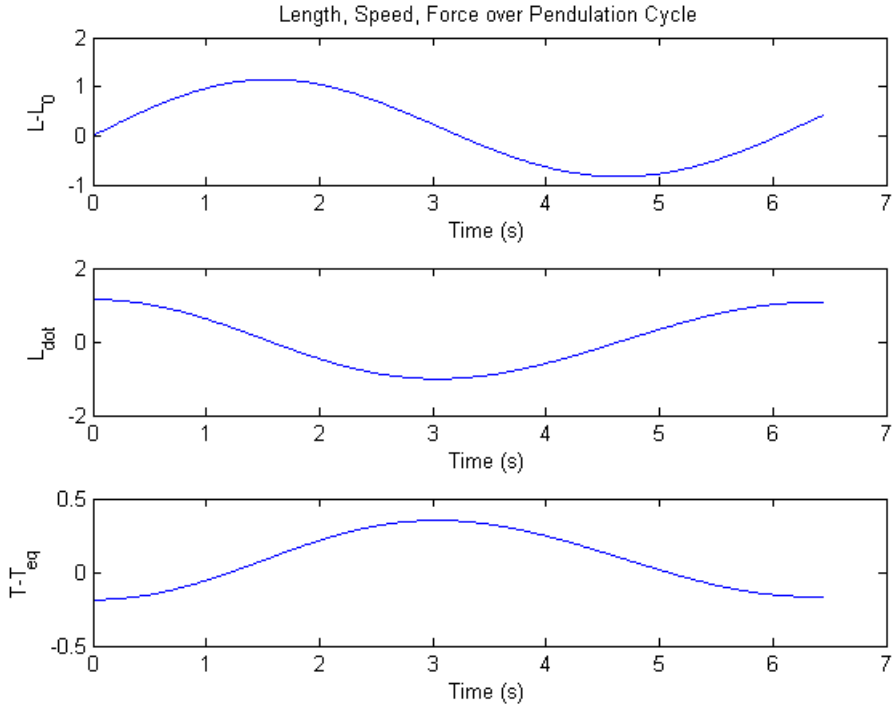

Figure 6.8: Length, speed, and force vs time for one pendulation cycle.

Dissipative work for one cycle is given by Equation 6.21.

$$W = \oint T dl \tag{6.21}$$

Figure 6.9 plots $T - T_{eq}$ vs $L - L_0$ for each point in time over the same pendulation cycle. Integrating over the cycle gives the dissipative work done by the winch. The winch dissipates roughly 2.7*percent* of the energy initially in the system after the first cycle.

$$W = 0.808J \tag{6.22}$$

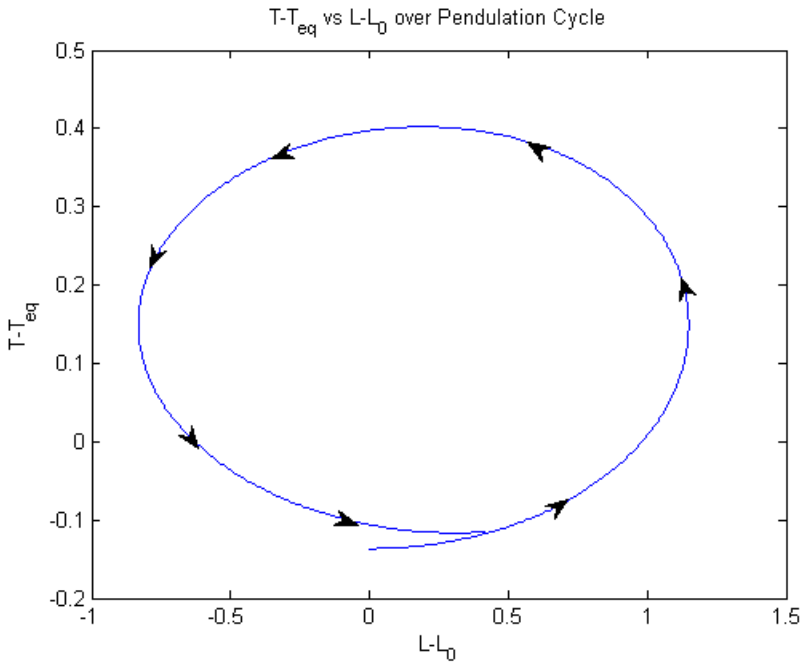

Figure 6.9: Hysteresis plot showing dissipative work done by winch.

For a simulation with a base winch speed of $\dot{l_0} = 0.5m/s$ and initial payload angle of $\theta_0 = 10degrees$, tether length is plotted vs time. Figure 6.10 shows the modulated motion of the tether over the duration of the hoist.

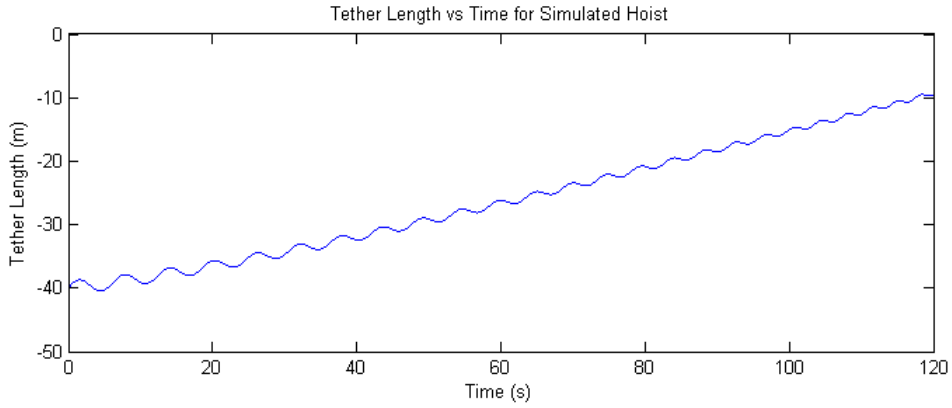

Figure 6.10: Tether Length vs time for simulated hoist.

To understand the effect of gross winch speed on payload sway control, several simulations were conducted at speeds varying from $\dot{l}_0 = 0m/s$ to $\dot{l}_0 = 0.5m/s$. For each simulation, percent reduction in deflection is measured after 6 pendulum cycles and given in Table 6.1. As the table shows, deflection is reduced a greater amount at higher gross winch speeds.

Table 6.1: Effect of base winch speed on percent reduction of $x_{deflection}$

$\dot{l}_0 = 0m/s$	Percent Reduction $x_{deflection}$
0.0	24.7701
0.1	30.1437
0.2	35.7759
0.3	41.3506
0.4	48.1609
0.5	53.0747

6.3.4 Effect of Sensor Noise on Sway Control

It is important that the controller performs under less than ideal feedback conditions. The actual tension feedback contains noise, which may affect the performance of the controller. Figure 6.11 shows tension feedback data from a suspended payload. A Discrete Fourier Transform, shown in figure 6.12, is used to identify frequencies with significant noise. The signal contains $25Hz$ noise of magnitude $\pm 15 percent$ of the DC value. This noise source is a result of the vibration of the load cell in line with the sensor. At other frequencies, magnitudes up to $\pm 5 percent$ of DC value appear. Vibration of various mechanical components of the payload are the likely contributors.

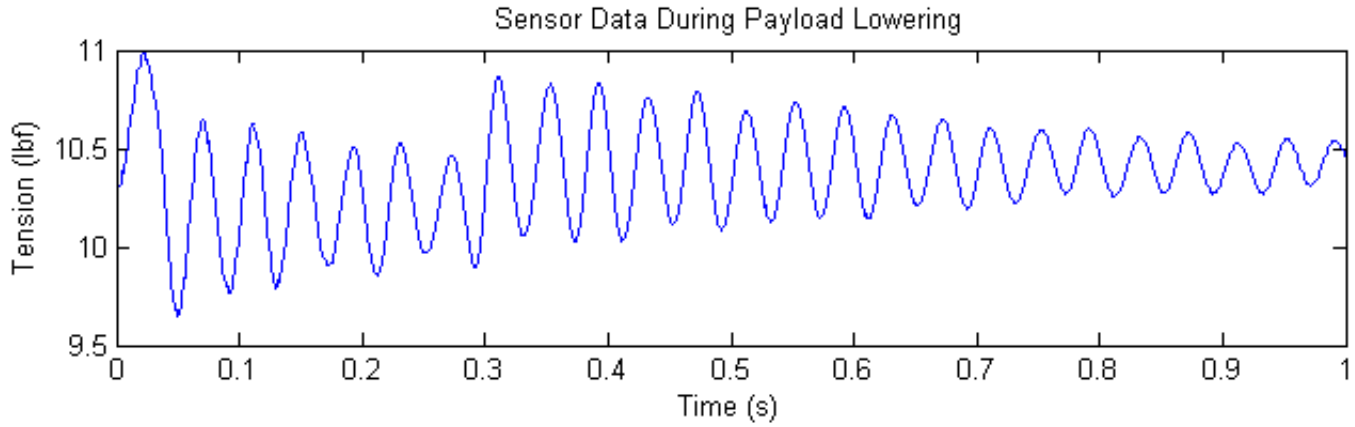

Figure 6.11: Tension feedback from LC103 load cell.

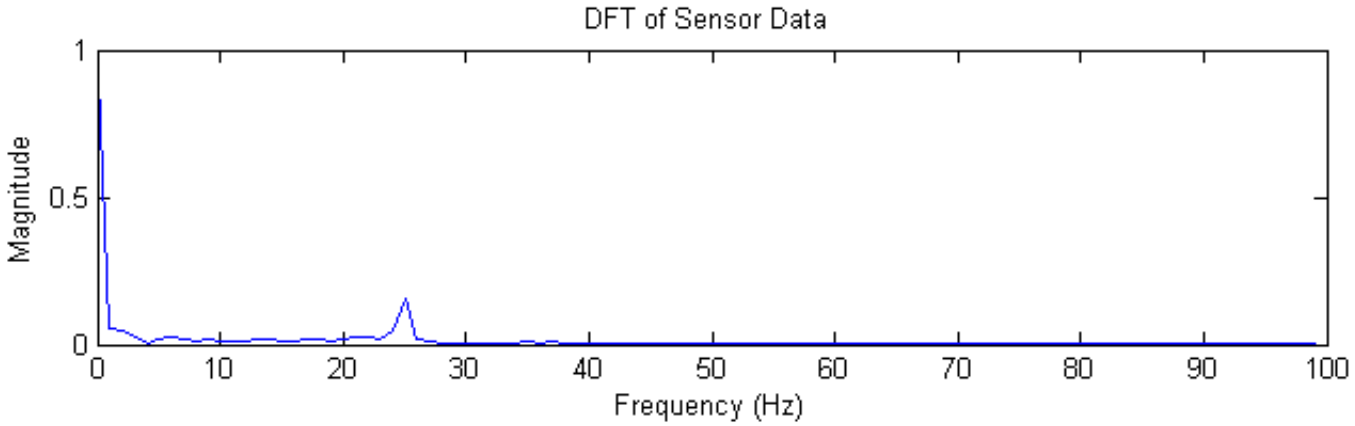

Figure 6.12: Discrete Fourier Transform of feedback data.

It is necessary to test the controller with noise added to the feedback. In order to test this conservatively, two sources are added to the sensor model in simulation. A $25Hz$ sine wave of magnitude $1.5lb$ and a random signal of $0.5lb$ are added to the ideal force measurement. These components account for the noise observed in the sensor data. The simulation is run, again with initial angle conditions $\theta_0 = 5$, $\theta_0 = 10$, $\theta_0 = 15$. Again, $\dot{theta}_0 = 0$ and $\dot{l}_0 = 0.2$.

Figure 6.13 shows the simulated hoist with sensor noise accounted for in the model. It is demonstrated that the noisy sensor data has little effect on the performance of the sway controller.

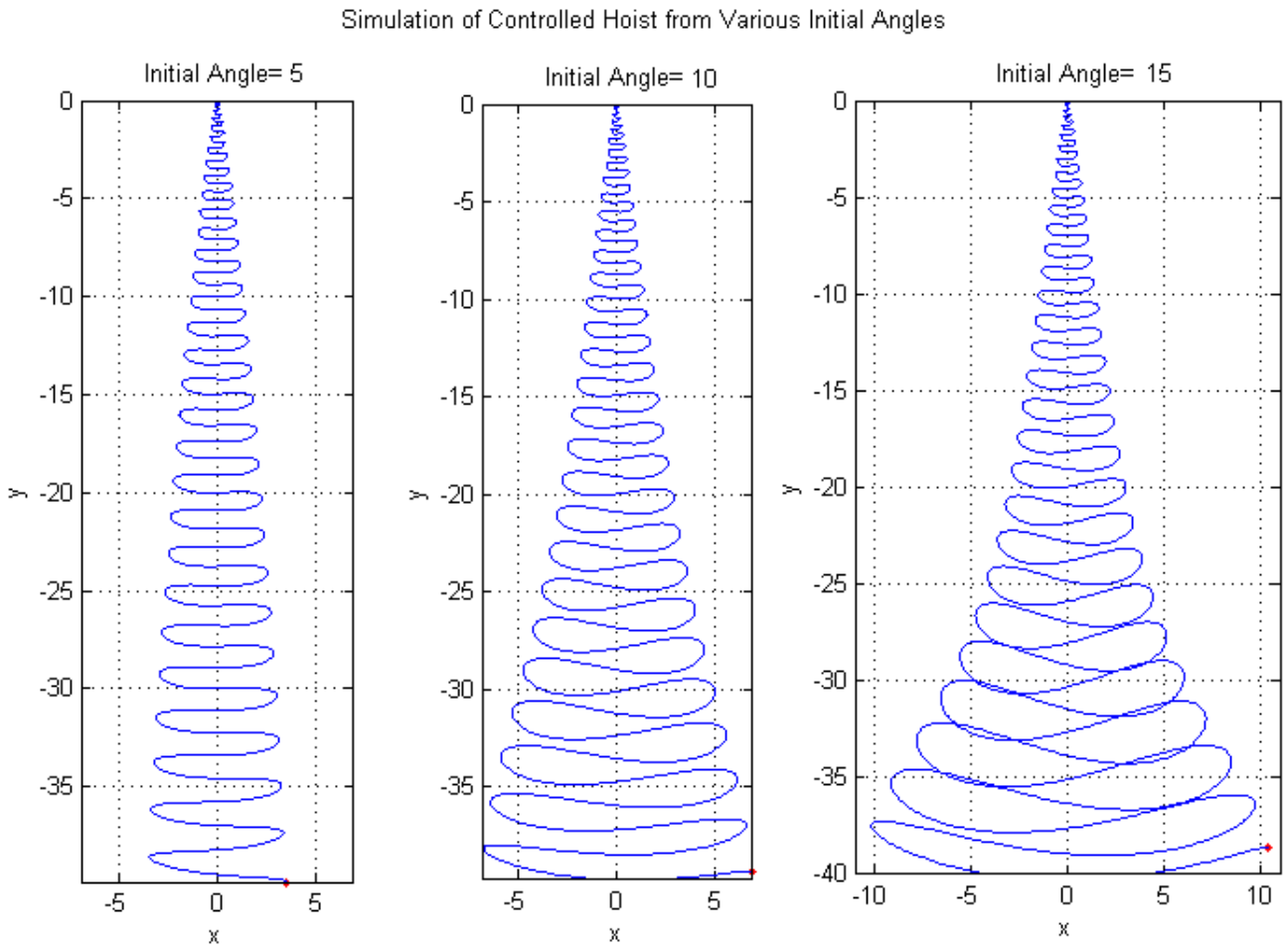

Figure 6.13: Simulation results controlled hoists with ideal and noisy sensor models.

6.4 Recommendations for Hardware Implementation

Simulation of the payload sway controller shows promising results. The next step will be to implement and test this controller on the hardware platform. In order to implement this controller on the actual system hardware, the following steps should be taken.

1. Redundant control of the brake switch should be implemented such that a failure in the SCU does not result in catastrophic system failure. This can be accomplished by adapting a radio controlled emergency stop switch to the existing circuitry. This will allow emergency brake control from the SCU and from a designated safety official.

2. A tether release mechanism must be implemented as a precaution against brake failure. Again, redundant control is recommended.

3. The damping control algorithm must converted from Simulink dataflow language to a LabVIEW VI and downloaded to the SCU. A user interfase should be created and should feature a panel of commands and safety features.

6.5 Conclusions

The control approach investigated in this chapter appears to be an effective and robust method for reducing payload pendulations. The system dynamics and control principles are explained in detail. A method for optimizing the key control variable is introduced.

The controller is tuned accordingly and simulated under a variey of operating conditions. Significant noise is introduced to the sensor feedback, and the controller maintains its good performance. Recommendations are made for later implementation of this controller on the hardware platform.

Chapter 7

Conclusion and Recommendations

In order to lay the groundwork for future research in autonomous tethered payload deployment, the work summarized in this thesis has provided the following:

1. A first iteration, complete working teleoperated hardware system is in place for mechanical testing and evaluation of control algorithms. This system integrates off the shelf technology with custom electronics. Additionally, the system is expandable, so that testing of additional sensors can be achieved without a system redesign.

2. Electrical hardware has been designed and tested for instrumentation and sampling of tension feedback. This hardware is packaged on a small, low profile PCB and features low noise power regulation for the onboard integrated circuits and the tension sensor.

3. A control architecture is established for accomplishing tension control during ground

operations and sway control during hoists. Within this architecture, low level controllers have been designed, simulated, and tested on physical hardware. These controllers meet the bandwidth demands of the high level algorithms.

4. A tension controller has been devised, tested on hardware, and evaluated. The controller is effective in controlling line tension from initial conditions of descent and slack. This meets the design requirements established for the controller.

5. An adaptive sway controller has been investigated and simulated for the damping of payload oscillations during hoists and hovers. The theory behind this controller is derrived and explained. A technique for optimizing this controller is discussed.

The results of this work are encouraging, and researchers at Virginia Tech are ready to take the next steps towards its goal of deploying a tethered ground robot from an autonomous aerial platform. From this work, several recommendations can be made for future iterations of a hardware system design.

1. Currently the tension feedback sensor is mounted in line with the tether near the connection point of the ground robot. In this configuration, it is sampled, converted to an RS232 message, and transmitted to the System Control Unit via a $2.4GHz$ wireless link. A design is proposed where the tension controller is mounted onboard the pod, within a network of pulleys, which the tether is guided through. This will reduce measurement noise and eliminate a potential failure point in the wireless link.

Additionally, it will save two stages of data conversion, as the System Control Unit can read directly over a Serial Peripheral Interfase.

2. Once Item 1 has been addressed, the onboard electronics can be consolidated. The Load Cell Instrumentation Board can be integrated into the System Control Unit, where it is sampled and read directly. Because the Elmo Whistle was proven to be an effective motor controller, it too can be incorporated into the design of the System Control Unit. The Whistle is also sold as a PCB mount item. Consolidating all onboard electronics onto a single PCB or a PCB stack has obvious advantages. Printed electrical traces are less likely to fail than soldered or crimped connector joints. Additionally, it is easier to ensure that all electronic devices share a common ground plane. Lastly, consolidation saves space on board the pod.

3. Before a funtional system is deployed, all safety conditions must be considered. An emergency tether release mechanism should be incorporated into the pod design. Depending on the eventual method of actuation, the device will more than likely already be supported by the System Control Unit. Servo-actuated or spring loaded devices can be easily interfaced, as the SCU features free peripheral PWM and GPIO outputs.

Bibliography

[1] M Rose. *Design of a Helicopter Deployable Ground Robotic System for Hazardous Environments*. Masters Thesis, Virginia Polytechnic Institute and State University, 2010.

[2] L.R. Lucassen and F.J. Sterk. Dynamic stability analysis of a hovering helicopter with a sling load. *Journal of the American Helicopter Society*, 10:6, 1965.

[3] M. Bisgaard, A. la Cour-Harbo, E.N. Johnson, and J.D. Bendtsen. Vision aided state estimator for helicopter slung load system. *17th IFAC Symposiumon Automatic Control in Aerospace*, 2007.

[4] M. Bisgaard. *Modeling, Estimation, and Control of Helicopter Slung Load System*. Aalborg University Department of Electronic Systems, 2008.

[5] S.K. Agrawal. Dynamics and Control of Helicopters With a Six-Cables Suspended Robot. *ASME Design Engineering Technical Conferences*, 2005.

[6] S.K. Agrawal. Dynamics and Control of A Helicopter Carrying A Payload Using A Cable-Suspended Robot. 2005.

[7] Ronen T. Rosen, A. and R. Raz. Active aerodynamic stabilization of a helicopter/sling-load system. In *International Conference on Rotorcraft Basic Research, 2 nd, College Park, MD*, 1988.

[8] Selisteanu D. Popescu D. Bobasu, E. and D. Sendrescu. Nonlinear Algorithms for the Adaptive Control of a Handling Crane. *WSEAS TRANSACTIONS ON SYSTEMS*, 4:1642–1649, 2005.

[9] Yamamoto M. Yanai, N. and A. Mohri. Feed-Back Control of Crane Based on Inverse Dynamics Calculation. *International Conference on Intelligent Robots and Systems*, 2001.

[10] EM Abdel-Rahman and AH Nayfeh. Pendulation reduction in boom cranes using cable length manipulation. *Nonlinear Dynamics*, 27(3):255–269, 2002.

[11] A. Bockstedte and E. Kreuzer. Hoisting Manipulation by Modal Coupling Control for Underactuated Cranes. *Solid Mechanics and Its Applications*, 130:121, 2005.

[12] Maxon motor specs. http://www.maxonmotorusa.com.

[13] Mcb2300 schematics. http://www.keil.com/mcb2300/mcb2300-schematics.pdf.

[14] Elmo motion control. http://www.elmomc.com.

[15] Ales. Tondl. *Autoparametric Resonance in Mechanical Systems.* Cambridge University Press, Cambridge, United Kingdom, 2000.

Appendix A

Electrical Schematics

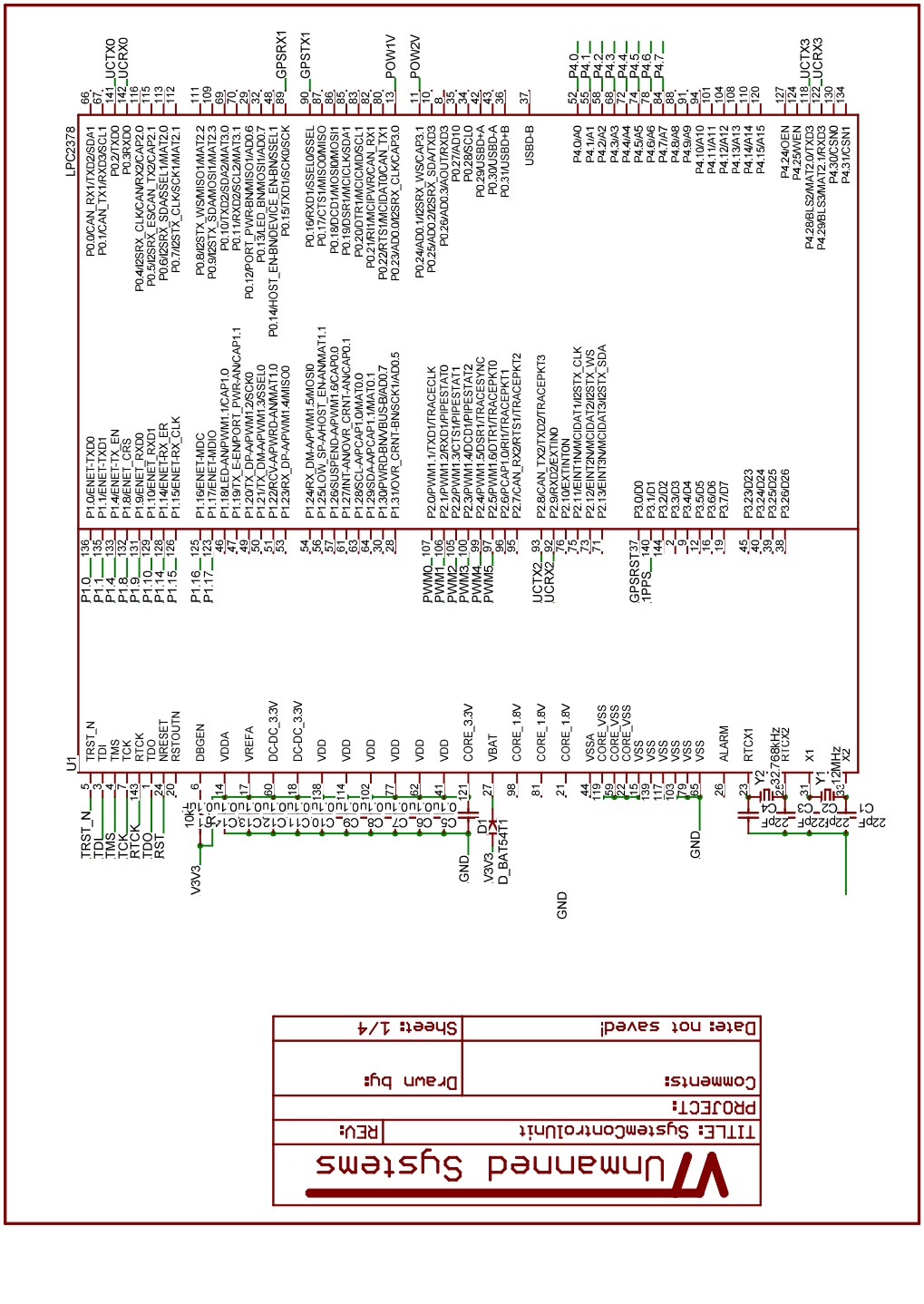

Figure A.1: System Control Unit schematic, page 1.

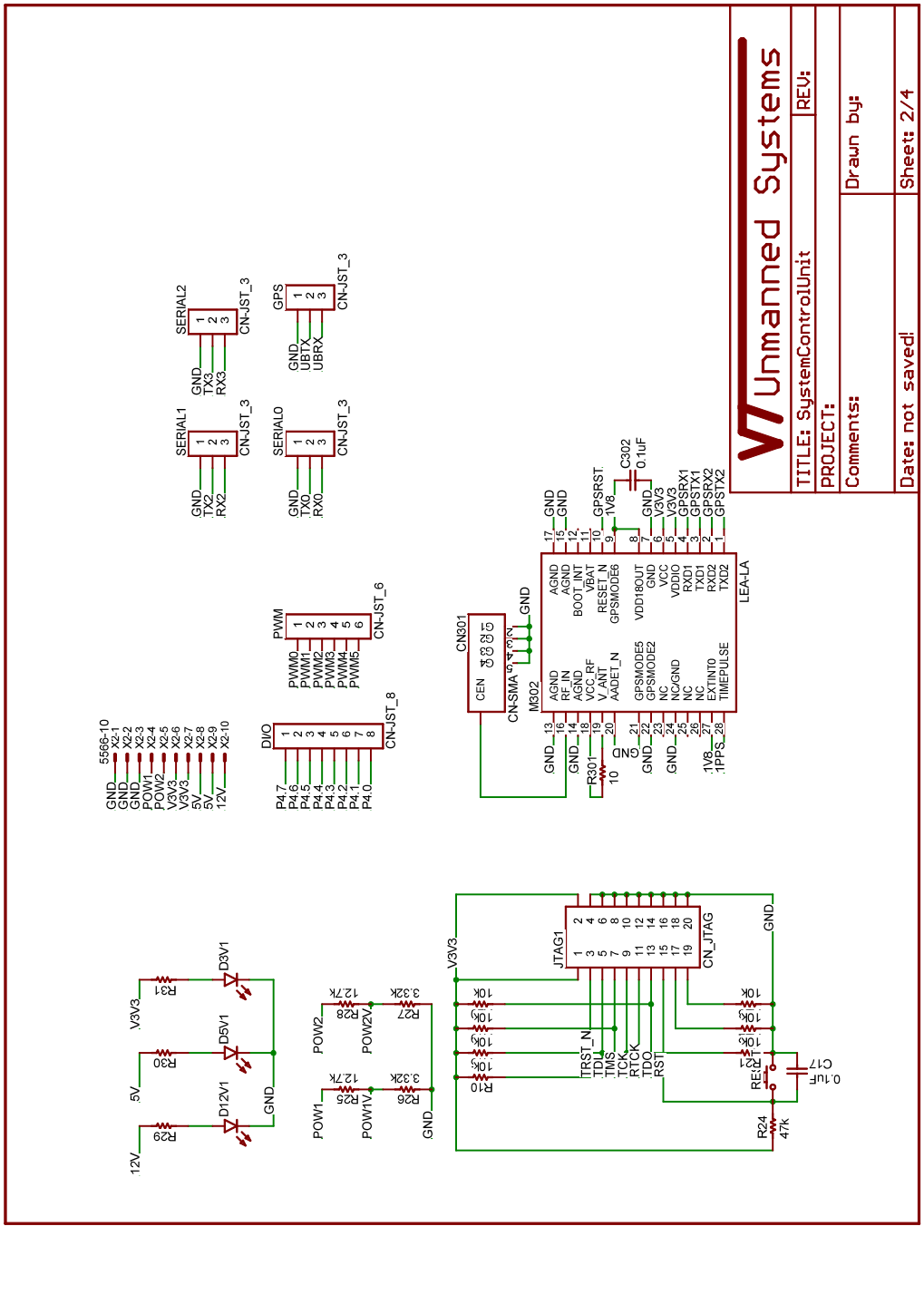

Figure A.2: System Control Unit schematic, page 2.

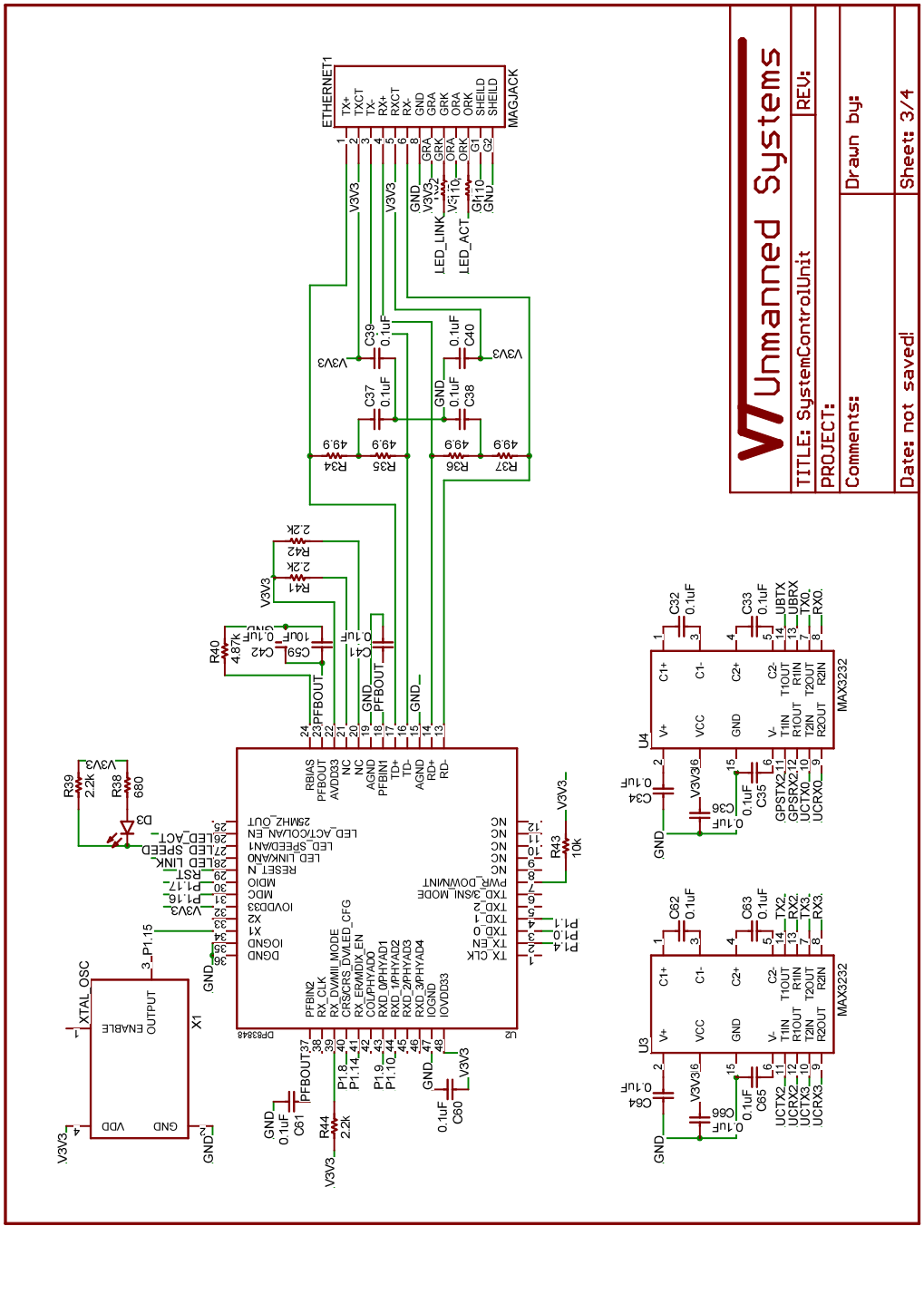

Figure A.3: System Control Unit schematic, page 3.

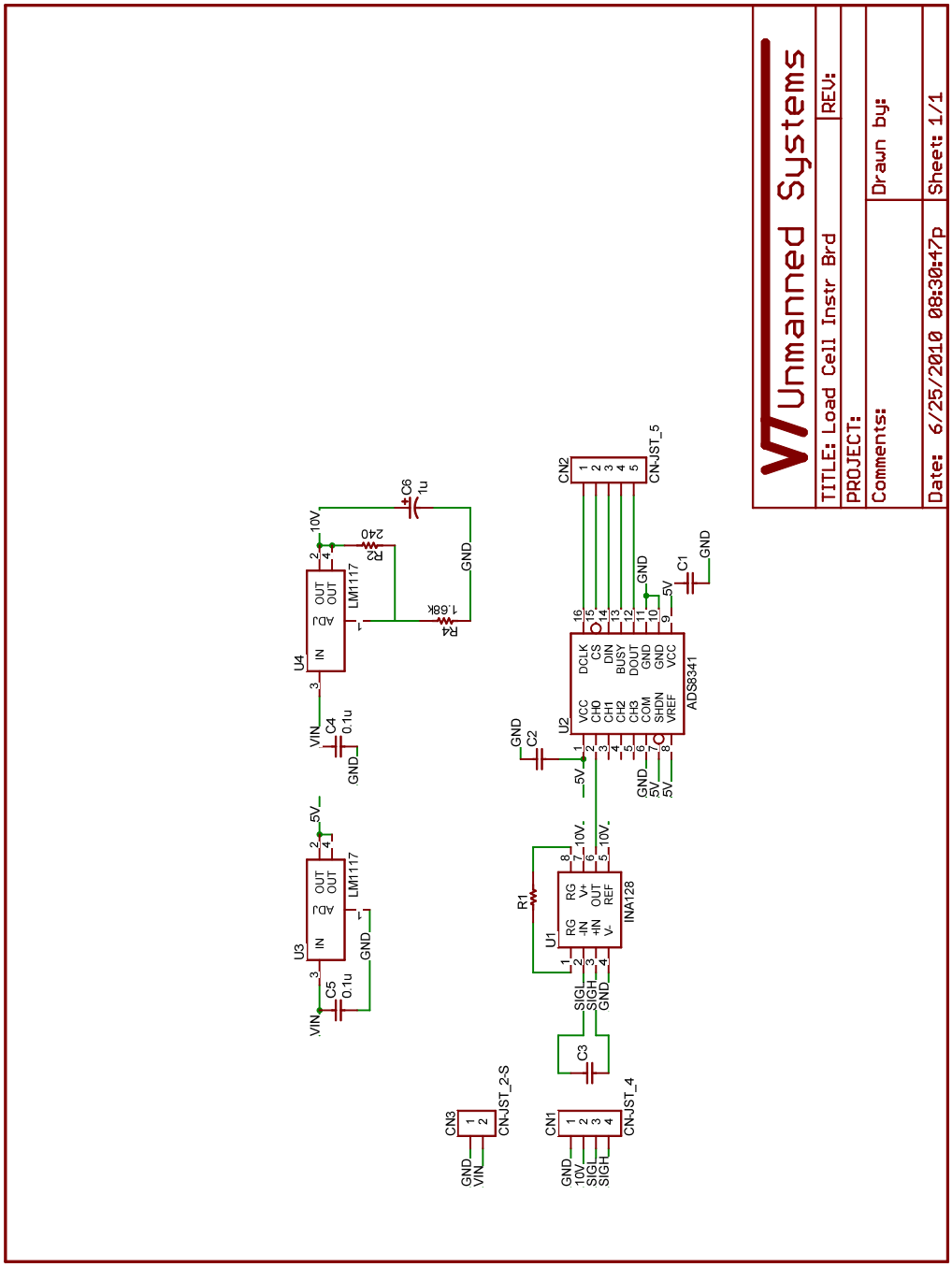

Instr Brd Sch.pdf